NUREG/CR--2134

DE83 900713

NUREG/CR-2134
EPRI NP-1582
GEAP-24940
R2

BWR Refill-Reflood Program, Task 4.7: Constitutive Correlations For Shear and Heat Transfer For the BWR Version of TRAC

Manuscript Completed: December 1981
Date Published: November 1982

Prepared by
J. G. M. Andersen, K. H. Chu

Nuclear Engineering Division
General Electric Company
San Jose, CA 95125

Prepared for
Division of Accident Evaluation
Office of Nuclear Regulatory Research
U.S. Nuclear Regulatory Commission
Washington, D.C. 20555
NRC FIN No. B5877

and
Electric Power Research Institute
3412 Hillview Avenue
Palo Alto, CA 94303

and
Nuclear Engineering Division
General Electric Company
San Jose, CA 95125

U. S. Nuclear Regulatory Commission

Previous Reports in BWR Refill-Reflood Program Series

BWR Refill-Reflood Program Task 4.1 - Program Plan, G. W. Burnette, General Electric Company, NUREG/CR-1972, January 1981.

BWR Refill-Reflood Program Task 4.2 - Core Spray Distribution Experimental Task Plan, T. Eckert, General Electric Company, NUREG/CR-1558, August 1980.

BWR Refill-Reflood Program Task 4.2 - Core Spray Distribution Final Report, T. Eckert, General Electric Company, NUREG/CR-1707, September 1980.

BWR Refill-Reflood Program Task 4.3 - Single Heated Bundle Experimental Task Plan, D. D. Jones, L. L. Myers, J. A. Findlay, General Electric Company, NUREG/CR-1788, January 1980.

BWR Refill-Reflood Program Task 4.3 - Single Heated Bundle Experimental Task Plan, Addendum I, Stage 3 - Separate Effects Bundle, D. D. Jones, General Electric Company, NUREG/CR-1708 - Add. I, July 1980.

BWR Refill-Reflood Program Task 4.4 - CCFL Refill System Effects Tests (30° Sector) Experimental Task Plan, D. G. Schumacher, General Electric Company, NUREG/CR-1846, December 1980.

BWR Refill-Reflood Program Task 4.4 - CCFL Refill System Effects Tests (30° Sector) Experimental Task Plan, Addendum A, SSTF CCFL/Refill Shakedown Plan, D. G. Schumacher, General Electric Company, NUREG/CR-1846, April 1981.

BWR Refill-Reflood Program Task 4.4 - CCFL Refill System Effects Tests (30° Sector) Experimental Task Plan, Addendum B, 30° SSTF CCFL/Refill Separate Effects Test Plan, D. G. Schumacher, General Electric Company, NUREG/CR-1846, April 1981.

BWR Refill-Reflood Program Task 4.4 - CCFL Refill System Effects Tests (30° Sector) Experimental Task Plan, Addendum C, BWR/6 System Response Test Plan, D. G. Schumacher, General Electric Company, NUREG/CR-1846, October 1981.

BWR Refill-Reflood Program Task 4.4 - 30° Sector SSTF Facility Description Document, J. E. Barton, D. G. Schumacher, J. A. Findlay and S. C. Caruso, General Electric Company, NUREG/CR-2133, June 1981.

BWR Refill-Reflood Program Task 4.7 - Model Development Task Plan, J. G. M. Andersen, B. S. Shiralkar, General Electric Company, NUREG/CR-2057, March 1981.

BWR Refill-Reflood Program Task 4.7 - TRAC/BWR Component Development, M. M. Aburomia, General Electric Company, NUREG/CR-2135, March 1981.

BWR Refill-Reflood Program Task 4.8 - Model Qualification Task Plan, J. A. Findlay, General Electric Company, NUREG/CR-1899, January 1981.

NUREG/CR-2134
EPRI NP-1582
GEAP-24940
DECEMBER 1981

BWR REFILL-REFLOOD PROGRAM
CONTRACT NO. NRC-04-79-184
AND EPRI PROJECT NO. RP1377-1

TASK 4.7 - CONSTITUTIVE CORRELATIONS FOR SHEAR AND HEAT TRANSFER FOR THE BWR VERSION OF TRAC

J. G. M. Andersen
K. H. Chu

Approved:
B. S. Shiralkar, Manager
Thermal Hydraulic Methods

Approved:
J. C. Black, Manager
External Programs

Approved:
G. E. Dix, Manager
Safety & Thermal
Hydraulic Technology

Approved:
J. E. Wood, Manager
Core Methods & Analysis

NUCLEAR ENGINEERING DIVISION • GENERAL ELECTRIC COMPANY
SAN JOSE, CALIFORNIA 95125

GENERAL ELECTRIC

CONTENTS

ILLUSTRATIONS

TABLES

ABSTRACT

TRAC (Transient Reactor Analysis Code) is a computer code for best estimate analysis of the thermal hydraulic conditions in a reactor system. The constitutive correlations for shear and heat transfer in the boiling water reactor (BWR) version of TRAC are described.

A new model, that accounts for the effect of phase and velocity profiles, has been developed for the interfacial shear and a new set of constitutive correlations are derived. Improvements have been made to the heat transfer in the area of subcooled boiling, boiling transition, and thermal radiation.

SUMMARY

TRAC (Transient Reactor Analysis Code) is a computer code for a best-estimate analysis of the thermal hydraulic conditions in a reactor system. As part of the development of a BWR version of TRAC, improvements and new models have been developed for the constitutive correlations for wall and interfacial shear and for wall and interfacial heat transfer.

A new model for the interfacial shear has been developed. The model accounts for the effect of phase and velocity profiles. Correlations for the interfacial shear and the distribution parameter have been developed for cocurrent flow from void fraction data, and for counter-current flow the correlations are in agreement with counter-current flow limitation (CCFL) data.

Improvements have been made to the heat transfer correlations in TRAC. A subcooled boiling model has been developed, a boiling length correlation has been introduced for critical heat flux, and a new correlation for the minimum point on the boiling curve has been included. Particular attention has been directed toward the heat transfer during emergency core coolant injection, and a model for thermal radiation heat transfer has been developed. This model accounts for both the surface-to-surface radiation and the interaction with the two-phase flow. A complete survey of the heat transfer models in the BWR version TRAC is given.

Finally, areas are reviewed where further improvements to the constitutive correlations are appropriate.

Section 1

INTRODUCTION

TRAC (Transient Reactor Analysis Code) is a computer code for best-estimate (BE) analysis of the thermal hydraulic conditions in a reactor system. Current development is concentrated on conditions following a loss of coolant accident (LOCA). TRAC was originally developed by the Los Alamos Scientific Laboratory for the analysis of pressurized water reactors (PWR) (1). The development of a boiling water reactor (BWR) version of TRAC was initiated in 1979.

A key feature of TRAC is a high degree of modularity and a stable numerical method. TRAC thus provides a framework where models for individual reactor components and physical phenomena can easily be interchanged. Furthermore, the free specification of the geometry allows the simulation of almost any geometry ranging from simple basic phenomena tests through system performance tests to complicated reactor systems. Consequently, the TRAC framework is a good base, around which a best estimate BWR code can be developed.

Two major tasks exist in the development of a BWR version of TRAC under the BWR Refill-Reflood Program:

- Development of models for the typical BWR components such as the fuel bundles, jet pump, steam separator, steam dryer, and the upper plenum.
- Development of models for the basic physical phenomena in a BWR, such as the heat transfer and the shear due to the walls and the interaction between the phases.

This report describes the second task, the development of models for the basic physical phenomena in a BWR. The development of models for BWR components are described separately (2).

The basic physical phenomena are described by constitutive correlations for the heat and mass transfer and the shear. Heat transfer occurs at the wall and at the interfaces, which together with a jump condition, describe the evaporation and condensation. The heat transfer includes convective and radiative heat transfer. The shear

stresses include the wall friction and the interaction between the phases, which are composed of drag, shear, and virtual mass effects.

The constitutive correlations for the shear and heat transfer are dependent on the flow regimes, and have been developed for each flow regime. The flow regimes considered in the BWR version of TRAC are:

- Single phase liquid flow
- Bubbly/Churn flow
- Annular flow
- Dispersed annular flow
- Inverse annular flow
- Single-phase steam flow
- Stratified flow in the vessel plena.

The flow regime map provides the logic used to determine which flow regime is present and, consequently, which correlation for the shear and heat transfer is to be used. Specific attention is not directed to the flow regime map, but together with the correlation for the shear and heat transfer, the logic for the selection of the individual correlations will be described.

In Section 2, the basic equations in TRAC are reviewed and the constitutive correlations for the shear and heat transfer are defined. Section 3 describes the model for the interfacial shear and wall friction, and the correlations which are used. Section 4 describes the heat transfer. Finally, Section 5 contains a discussion of the correlations and identifies the areas where further improvements are appropriate.

The models described in this report are included in the GE working version TRACB01, and have been made available to Idaho National Engineering Laboratory (INEL) for inclusion in the official INEL versions of TRAC-BD.

Section 2

BASIC EQUATIONS AND CONSTITUTIVE CORRELATIONS

The basic equations are the conservation equations for mass, momentum, and energy for each phase. In the BWR version of TRAC, the conservation equations are as follows:

- Mass:

$$\frac{\partial}{\partial t}(\alpha\rho_g) + \nabla \cdot (\alpha\rho_g \vec{V}_g) = \Gamma \tag{2-1}$$

$$\frac{\partial}{\partial t}[(1-\alpha)\rho_\ell + \alpha\rho_g] + \nabla \cdot [(1-\alpha)\rho_\ell \vec{V}_\ell + \alpha\rho_g \vec{V}_g] = 0 \tag{2-2}$$

- Momentum:

$$\frac{\partial}{\partial t}\vec{V}_g + \vec{V}_g \cdot \nabla\vec{V}_g + k\frac{\rho_c}{\alpha\rho_g}\left[\frac{\partial}{\partial t}(\vec{V}_g - \vec{V}_\ell) + \vec{V}_{di} \cdot \nabla(\vec{V}_g - \vec{V}_\ell)\right.$$

$$\left. - \frac{1}{\rho_g}\nabla P + \vec{g} - \frac{f_{\ell g}}{\alpha\rho_g} - \frac{F_{wg}}{\alpha\rho_g} = 0 \right. \tag{2-3}$$

$$\frac{\partial}{\partial t}\vec{V}_\ell + \vec{V}_\ell \cdot \nabla\vec{V}_\ell - k\frac{\rho_c}{(1-\alpha)\rho_\ell}\left[\frac{\partial}{\partial t}(\vec{V}_g - \vec{V}_\ell) + \vec{V}_{di} \cdot \nabla(\vec{V}_g - \vec{V}_\ell)\right]$$

$$- \frac{1}{\rho_\ell}\nabla P + \vec{g} + \frac{f_{\ell g}}{(1-\alpha)\rho_\ell} - \frac{F_{w\ell}}{(1-\alpha)\rho_\ell} = 0 \tag{2-4}$$

- Energy:

$$\frac{\partial}{\partial t}(\alpha\rho_g e_g) + \nabla \cdot (\alpha\rho_g e_g \vec{V}_g) = -P\left[\frac{\partial\alpha}{\partial t} + \nabla \cdot (\alpha\vec{V}_g)\right]$$

$$+ q'''_{wg} + q'''_{ig} + \Gamma h_{sg} \tag{2-5}$$

$$\frac{\partial}{\partial t}\left((1-\alpha)\rho_\ell e_\ell + \alpha \rho_g e_g\right) + \nabla \cdot \left((1-\alpha)\rho_\ell e_\ell \vec{V}_\ell + \alpha \rho_g e_g \vec{V}_g\right) =$$

$$+ q'''_{wg} + q'''_{w\ell} - P\nabla \cdot \left[(1-\alpha)\vec{V}_\ell + \alpha \vec{V}_g\right] \qquad (2\text{-}6)$$

A number of assumptions have been made in these equations, both in the original formulation of the equations (1) and in the formulation adopted for the BWR version of TRAC.

In the above equations, it has been assumed that each phase has the same pressure and that this pressure is the same as the interface pressure. This is in most cases a reasonable assumption, because the difference between the pressures is small. It may, however, have an effect on the stability of the numerical method applied for the solution of the equations. Only in the case of stratification due to gravity can the difference between the phase pressures be significant; e.g., the above formulation does not allow counter-current flow in a horizontal pipe.* The difference between the pressures of each phase can be simulated by adding the following terms to the right-hand side of the vapor and liquid momentum equations:

$$\frac{1}{2}\frac{\Delta\rho}{\rho_g} g_v \nabla_h \alpha \qquad (2\text{-}7)$$

and

$$-\frac{1}{2}\frac{\Delta\rho}{\rho_\ell} g_v \nabla_h \alpha \qquad (2\text{-}8)$$

Here g_v is the vertical component of the gravity vector and $\nabla_h \alpha$ is the horizontal component of the void fraction gradient. For details on the derivation of this term, see Appendix A.

In the momentum equations, the shear tensor** and the exchange of momentum due to evaporation*** have been omitted. The shear tensor is usually small compared to the

---

*This flow pattern would not normally happen in a BWR unless liquid entered the steam line.

**The development of a model for the turbulent shear and mixing in the upper plenum is currently underway.

***This source term appears in the TRAC manual (1), but an examination of the source deck indicates that the term has been omitted, and consequently it has been omitted from the above equations. The term is generally small compared to the rest of the terms in the momentum equation.

wall friction. Only in the upper plenum will the term be significant, as it influences the amount of mixing and thereby the subcooled countercurrent flow (CCFL) breakdown. In the momentum equation, however, a term that represents the interaction with the wall has been included. This term will represent the part of the shear that is due to wall friction. Furthermore, in the momentum equation the virtual mass effect has been included.

In the energy equation, the gravity term and the dissipation energy have been neglected. The first is insignificant, but the latter may be important for the pumps or for critical flow and should be included.

Finally, it is worth noting that only the continuity equations are of a conserving form. The momentum equations, which are really the equations of motion, are not conserving at all, and the energy equations are not conserving since the kinetic and potential energy have been eliminated from the equations and the dissipation has been neglected. If the kinetic and potential energy or the dissipation is important, an error in the energy balance will appear. This is usually of no importance for BWR transients.

The constitutive correlations, which are necessary for the closure of the equations and which will be described in the following sections, are as follows:

k = The magnitude of the virtual mass coefficient

ρ_c = The density of the continuous phase

V_{di} = The velocity of the dispersed phase

$f_{\ell g}$ = The interfacial shear and drag

$F_{w\ell}$ = Wall friction on the liquid

F_{wg} = Wall friction on the vapor

q'''_{ig} = The interface-to-vapor heat transfer per unit volume

$q'''_{i\ell}$ = The interface-to-liquid heat transfer per unit volume

q'''_{wg} = The wall-to-vapor heat transfer per unit volume

$q'''_{w\ell}$ = The wall-to-liquid heat transfer per unit volume

The evaporation or condensation is given by the jump condition for the interface

$$\Gamma = - \frac{q'''_{i\ell} + q'''_{ig}}{h_{\ell g}} \qquad (2\text{-}9)$$

Section 3

INTERFACIAL SHEAR AND WALL FRICTION

The bulk of the data available for the evaluation of the interfacial shear and the wall friction are void fraction and pressure drop data. These are also the parameters that are important and must be described accurately in a best estimate analysis of the two-phase flow in a BWR.

More fundamental data are available for the shear and the interfacial forces, and much basic research is going on. However, a comprehensive set of models for the shear and interfacial forces for all flow regimes does not presently exist, and the ones that do exist are primarily for idealized flow regimes. Furthermore, little information is presently available on the phase and flow distributions which, as it turns out, have a significant effect on the void fraction or the relative velocity. For these reasons we have chosen to base the development of constitutive correlations for the interfacial shear on the very large data base that exists for void fractions and pressure drops. The correlations will be based on the following:

- Theorem – For adiabatic and steady-state conditions, the two-fluid model and the drift flux model are equivalent, and the drift flux parameters can be used to characterize the relative velocity and the phase and flow distributions.

- Assumption – The correlations for the interfacial shear and drag, and wall friction, as derived from adiabatic steady-state conditions, are applicable for transient conditions.

In the following sections a relationship between the interfacial shear and the drift flux parameters, will be developed, and correlations for the interfacial shear for various flow regimes will be derived.

3.1 SHEAR AND WALL FRICTION

The presence of wall friction creates a shear field in the two-phase flow. This shear field will interact with both phases, and thus create an interfacial force, which has its origin in the wall friction.

For example, for steady-state bubbly flow, the momentum equations can be written as

$$0 = -\alpha \frac{\partial P}{\partial z} - \alpha \rho_g g - f_{\ell g} \text{ , for the vapor}$$

$$0 = -(1-\alpha) \frac{\partial P}{\partial z} - (1-\alpha)\rho_\ell g + f_{\ell g} - F_w \text{ , for the liquid}$$

where $f_{\ell g}$ represents the shear at the interface, and F_w represents the shear between the wall and the liquid. If the pressure gradient is eliminated from the above equations, one obtains

$$f_{\ell g} = (\rho_\ell - \rho_g) g\, \alpha(1-\alpha) + \alpha F_w$$

Consequently if the interfacial shear above was a function only of the relative velocity between the phases, the relative velocity would be dependent upon the wall friction or the Reynolds number. This, however, is not the case. Data (3,4) indicate that the drift velocity is virtually independent of the flow rate. The interfacial shear, therefore, besides a term that is a function of the relative velocity, consists of another term with its origin in the wall friction.

Following Ishii's notation (3) the local time-averaged momentum equations for the gas and liquid phases are

$$\alpha \rho_g \left(\frac{\partial \vec{V}_g}{\partial t} + \vec{V}_g \cdot \nabla \vec{V}_g \right) = -\alpha \nabla P + \alpha \nabla \cdot \bar{\bar{\tau}} - \alpha \rho_g \vec{g} - M_g \qquad (3\text{-}1)$$

$$(1-\alpha)\rho_\ell \left(\frac{\partial \vec{V}_\ell}{\partial t} + \vec{V}_\ell \cdot \Delta \vec{V}_\ell \right) = -(1-\alpha)\Delta P + (1-\alpha)\nabla \cdot \bar{\bar{\tau}} - (1-\alpha)\rho_\ell \vec{g} - M_\ell \qquad (3\text{-}2)$$

Here the interfacial mass transfer and the virtual mass effect have been neglected, and M must obey

$$M_g + M_\ell = 0 \qquad (3\text{-}3)$$

For one-dimensional flow, Eqs. 3-1 and 3-2 degenerate to

$$\alpha \rho_g \left(\frac{\partial V_g}{\partial t} + V_g \frac{\partial V_g}{\partial z} \right) = -\alpha \frac{\partial P}{\partial z} + \alpha \nabla \cdot \bar{\bar{\tau}}_z - \alpha \rho_g g - M_g \qquad (3\text{-}4)$$

$$(1-\alpha)\rho_\ell \left(\frac{\partial V_\ell}{\partial t} + V_\ell \frac{\partial V_\ell}{\partial z}\right) = - (1-\alpha) \frac{\partial P}{\partial z} + (1-\alpha) \nabla \cdot \bar{\bar{\tau}}_z - (1-\alpha)\rho_\ell g + M_g \qquad (3\text{-}5)$$

An interpretation of the various terms on the right hand side of Eqs. 3-4 and 3-5 can be obtained from Figure 3-1.

For the gas equation the interpretation of the various terms are as follows:

$- \alpha \frac{\partial P}{\partial z}$ = the force on the gas due to the pressure gradient in the z direction (the pressure is assumed to be the same for each phase)

$\alpha \nabla \cdot \bar{\bar{\tau}}_z$ = the force on the gas due to the shear at the surface of the incremental volume (α is the fraction of the surface which is occupied by the gas). It is assumed that the averaged shear tensor is the same for each phase, which is reasonable, because, except for surface tension and mass transfer effects, the shear is a continuous function.

$- \alpha\rho_g g$ = the body force, due to gravity, on the gas.

M_g = the interfacial drag between the phases inside the incremental volume due to local difference in the phase velocities.

For adiabatic steady state conditions, Eqs. 3-4 and 3-5 reduce to

$$\alpha \frac{\partial P}{\partial z} - \alpha \nabla \cdot \bar{\bar{\tau}}_z + \alpha\rho_g g + M_g = 0 \qquad (3\text{-}6)$$

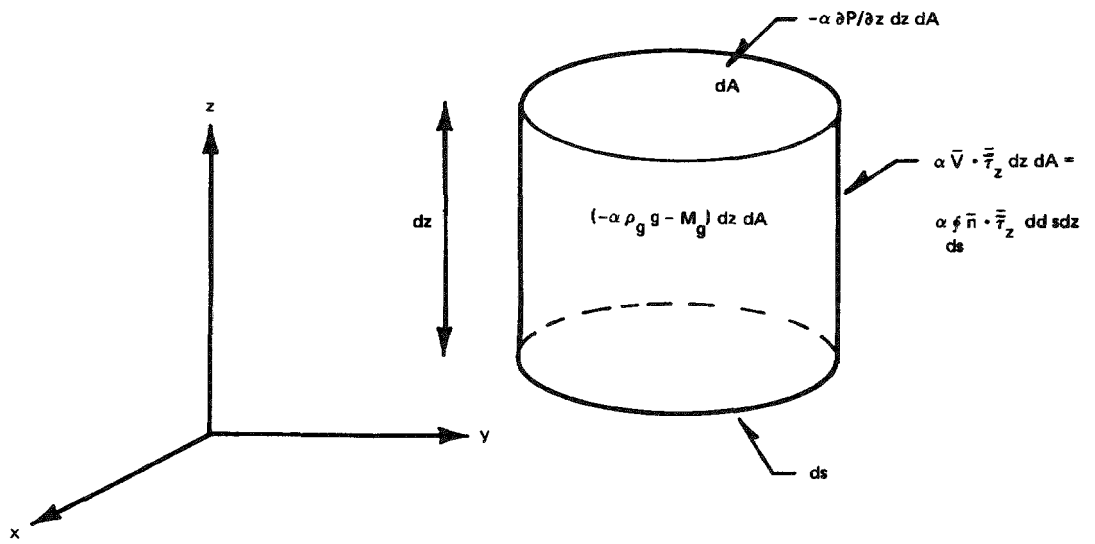

Figure 3-1. Right-Hand Side of Vapor Momentum Equation

$$(1-\alpha)\frac{\partial P}{\partial z} - (1-\alpha)\nabla \cdot \bar{\bar{\tau}}_z + (1-\alpha)\rho_\ell g - M_g = 0 \tag{3-7}$$

When Eqs. 3-6 and 3-7 are added,

$$\frac{\partial P}{\partial z} - \nabla \cdot \bar{\bar{\tau}}_z + ((1-\alpha)\rho_\ell + \alpha\rho_g)g = 0 \tag{3-8}$$

The integration of this equation over the cross section, assuming that the densities and the pressure gradient are constant across the flow area, results in

$$A\frac{\partial P}{\partial z} = \oint \bar{n} \cdot \bar{\bar{\tau}}_{wz}\, ds + A\,(\langle 1-\alpha\rangle\rho_\ell + \langle\alpha\rangle\rho_g)\, g = 0 \tag{3-9}$$

The integral is along the boundary (w), $\bar{n}$ is the normal to the boundary, and Gauss's theorem has been used. When Eqs. 3-8 and 3-9 are combined,

$$\nabla \cdot \bar{\bar{\tau}}_z = \frac{1}{A}\oint \bar{n} \cdot \bar{\bar{\tau}}_{wz}\, ds - \Delta\rho g\,(\alpha - \langle\alpha\rangle) \tag{3-10}$$

Integrating the momentum equation for the gas over the cross section results in

$$\langle\alpha\rangle A\frac{\partial P}{\partial z} - \int_A \alpha\nabla \cdot \bar{\bar{\tau}}_z\, dA + \langle\alpha\rangle A\rho_g\, g + \int_A M_g\, dA = 0 \tag{3-11}$$

The second term in this equation can be evaluated using Eq. 3-10:

$$\int_A \alpha\,\nabla \cdot \bar{\bar{\tau}}_z\, dA = \langle\alpha\rangle \oint \bar{n} \cdot \bar{\bar{\tau}}_{wz}\, dS - A\Delta\rho g \left\langle(\alpha-\langle\alpha\rangle)^2\right\rangle \tag{3-12}$$

The left side of Eq. 3-12 is the total amount of shear on the vapor phase. The first term on the right side is the void fraction times the wall friction. The second term is an induced shear stress due to the variance of the void fraction with the radius.

$$f_i = -A\,\Delta\rho\, g\, \left\langle(\alpha-\langle\alpha\rangle)^2\right\rangle \tag{3-13}$$

and from which

$$\int \alpha \nabla \cdot \bar{\bar{\tau}}_z \, dA = - \langle\alpha\rangle F_w - f_i \tag{3-14}$$

Inserting this into Eq. 3-11

$$\langle\alpha\rangle A \frac{\partial P}{\partial z} + \langle\alpha\rangle F_w + f_i + \langle\alpha\rangle A\rho_g g + \int_A M_g \, dA = 0 \tag{3-15}$$

Similarly, for the liquid momentum equation,

$$\langle 1-\alpha\rangle A \frac{\partial P}{\partial z} + \langle 1-\alpha\rangle F_w - f_i + \langle 1-\alpha\rangle A \rho_\ell g - \int_A M_g \, dA = 0 \tag{3-16}$$

The physical interpretation of the various terms in the integrated momentum equation for the gas are as follows:

$\langle\alpha\rangle A \frac{\partial P}{\partial t}$ = The force due to the pressure gradient.

$\langle\alpha\rangle F_w$ = Induced shear stress due to the shear created by the wall friction.

$\langle\alpha\rangle A\rho_g g$ = The body force due to gravity.

$\int_A M_g \, dA$ = The drag force between the phases due to local velocity differences.

f_i = Induced shear stress due to the radial phase distribution.

The terms in the integrated liquid momentum equation can, of course, be interpreted in the same way.

Consequently, if the liquid phase alone is in contact with the wall, the wall friction acts alone on the liquid, giving

$$F_g = 0$$

$$F_\ell = F_w$$

The induced shear, however, caused by the wall friction, creates an interfacial force between the phases given by

$$\langle\alpha\rangle F_w$$

and the net forces on the phases due to the wall friction become

$\langle\alpha\rangle F_w$, for the gas phase

$\langle 1-\alpha\rangle F_w$, for the liquid phase

Similarly, if the gas-phase is in contact with the wall,

$$F_g = F_w$$

$$F_\ell = 0$$

and the interfacial force, due to the wall friction, become

$$\langle 1-\alpha\rangle F_w$$

Again, the net forces on the phases due to the wall friction become

$\langle\alpha\rangle F_w$, for the gas phase

$\langle 1-\alpha\rangle F_w$, for the liquid phase

3.2 INTERFACIAL DRAG AND PHASE DISTRIBUTION

In Section 3.1, the interfacial force due to the wall friction was derived. The remaining interfacial forces then become a function of the interface drag due to the difference in the phase velocities, the buoyancy due to the gravity, and a force that is due to the phase distribution.

When $\partial P/\partial z$ and $\bar{\bar{\tau}}_z$ are eliminated from Eqs. 3-6 and 3-7,

$$M_g = \alpha\,(1-\alpha)\,\Delta\rho\; g \qquad (3\text{-}17)$$

The physical interpretation of this equation is that locally the drag is equal to the buoyancy. Integrating this equation over the cross section gives

$$\int M_g \, dA = A \, \Delta\rho \, g \, \langle\alpha(1-\alpha)\rangle \tag{3-18}$$

This equation combined with Eq. 3-13 gives the total interaction between the phases due to drag or shear

$$f_{\ell g} = f_i + \int_A M_g \, dA = A \, \Delta\rho \, g \, \langle\alpha\rangle\langle 1-\alpha\rangle \tag{3-19}$$

For fully dispered flow, from Eqs. 3-13 and 3-18

$$f_i = 0 \quad \text{and} \quad \int M_g \, dA = A \, \Delta\rho \, g \, \langle\alpha\rangle\langle 1-\alpha\rangle$$

The interaction is given by the drag between the phases. There is no shear between the phases, except for the term due to the wall friction.

For fully separated flow, e.g., annular flow,

$$f_i = A \, \Delta\rho \, g \, \langle\alpha\rangle\langle 1-\alpha\rangle \quad \text{and} \quad \int_A M_g \, dA = 0$$

The interaction is given by the shear at the interface. There is no local drag.

In either case or any combination, however, the total interaction between the phases, except for the forces due to the wall friction, is given by Eq. 3-19.

The interfacial force must be related to the velocity difference between the phases. It is conventional to define

$$f_{\ell g} = \overline{C}_i \, | \, \overline{V}_r \, | \, \overline{V}_r \tag{3-20}$$

For fully dispersed flow, the local drag can be given by a drag coefficient

$$M_g = \frac{1}{8} \frac{C_D}{d_i} \rho_c \, | \, V_r \, | \, V_r \tag{3-21}$$

where ρ_c is the density of the continuous phase, and d_i^{-1} is the interface area per unit volume. However, it should be noted that without additional assumptions only $\overline{C}_i = 1/8\ C_D/d_i\ \rho_c$ can be correlated from the data.

Integrating Eq. 3-20 over the cross section, remembering that the flow is dispersed, yields

$$\frac{1}{A} \int M_g\, dA = A\, \overline{C}_i' \mid \overline{V}_r \mid \overline{V}_r \tag{3-22}$$

where

$$\overline{V}_r = \frac{\langle f(\alpha)\ V_r \rangle}{\langle f(\alpha) \rangle} \tag{3-23}$$

$$\overline{C}_i' = \frac{\langle C_i \mid V_r \mid V_r \rangle \langle f(\alpha) \rangle^2}{\mid \langle f(\alpha)\ V_r \rangle \mid \langle f(\alpha)\ V_r \rangle} \tag{3-24}$$

and $f(\alpha)$ is a weighting function. For dispersed flow, the concentration of the dispersed phase would be a logical choice, and a function that meets this criterion for both $\alpha \to 0$ for bubbly flow and $\alpha \to 1$ for droplet flow is

$$f(\alpha) = \alpha\ (1-\alpha) \tag{3-25}$$

It is important to note that

$$\overline{V}_r \neq \overline{V}_g - \overline{V}_\ell \tag{3-26}$$

where

$$\overline{V}_g = \frac{\langle \alpha\ V_g \rangle}{\langle \alpha \rangle}$$

$$\overline{V}_\ell \quad \frac{\langle (1-\alpha)\ V_\ell \rangle}{\langle 1-\alpha \rangle}$$

$\overline{V}_g$ and $\overline{V}_\ell$ have different weight functions. Thus we will only have $\overline{V}_r = \overline{V}_g - \overline{V}_\ell$ for a uniform phase or velocity distribution. Using

$$V_r = \frac{V_{gj}}{1-\alpha}$$

inserting it into Eq. 3-23 and using Eq. 3-25 yields

$$\overline{V}_r = \frac{1}{\eta} \frac{\overline{V}_{gj}}{\langle 1-\alpha \rangle} \tag{3-27}$$

where

$$\overline{V}_{gj} = \frac{\langle \alpha\, V_{gj} \rangle}{\langle \alpha \rangle} \tag{3-28}$$

$$\eta \quad \frac{\langle \alpha(1-\alpha) \rangle}{\langle \alpha \rangle \langle 1-\alpha \rangle} \tag{3-29}$$

Combining Eqs. 3-22 and 3-27 yields

$$\frac{1}{A} \int_A M_g \, dA = \overline{C}_i' \frac{|\overline{V}_{gj}| \overline{V}_{gj}}{\eta^2 \langle 1-\alpha \rangle^2} \tag{3-30}$$

Furthermore, combining Eqs. 3-18 and 3-30 results in

$$\overline{C}_i \frac{|\overline{V}_{gj}| V_{gj}}{\langle 1-\alpha \rangle^2} = \Delta\rho g \langle \alpha(1-\alpha) \rangle \tag{3-31}$$

where

$$\overline{C}_i = \frac{1}{\eta^2} \overline{C}_i' \tag{3-32}$$

With V_{gj} correlated from void fraction data, C_i can be obtained from Eq. 3-31.

Using

$$\overline{V}_g = C_o \langle j \rangle + \overline{V}_{gj} \tag{3-33}$$

where

$$C_o = \frac{\langle \alpha\, j \rangle}{\langle \alpha \rangle \langle j \rangle} \tag{3-34}$$

and

$$\langle j \rangle = \langle 1-\alpha \rangle \bar{V}_\ell + \langle \alpha \rangle \bar{V}_g \tag{3-35}$$

and combining it with Eq. 3-27 gives

$$\bar{V}_r = \frac{1}{n}\left(\frac{1-\langle \alpha \rangle C_o}{\langle 1-\alpha \rangle} \bar{V}_g - C_o \bar{V}_\ell\right) \tag{3-36}$$

This expression combined with Eqs. 3-27, 3-30 and 3-32 results in

$$\frac{1}{A}\int M_g \, dA = \bar{C}_i \left| \frac{1-\langle \alpha \rangle C_o}{\langle 1-\alpha \rangle} \bar{V}_g - C_o \bar{V}_\ell \right| \left(\frac{1-\langle \alpha \rangle C_o}{\langle 1-\alpha \rangle} \bar{V}_g - C_o \bar{V}_\ell\right) \tag{3-37}$$

Thus, with C_o correlated from void fraction data, the interfacial drag for dispersed flow can be calculated.

For separated flow, the drift flux correlation, being based on local drag considerations, breaks down. For fully separated flow

$$\bar{V}_{gj} = \frac{\langle \alpha\, V_{gj} \rangle}{\langle \alpha \rangle} = 0$$

However, as discussed earlier, for fully separated flow the local drag is zero, and the interfacial force is given by the shear at the interface.

Correlating the interfacial shear in Eq. 3-13, as a function of the material properties and the average velocities results in

$$\frac{1}{A} f_i = C_i' \left| C_1 \bar{V}_g - C_2 \bar{V}_\ell \right| (C_1 \bar{V}_g - C_2 \bar{V}_\ell) \tag{3-38}$$

where C_i' is a friction coefficient, and C_1 and C_2 account for the effect of the velocity profiles.

Now defining and substituting

$$C_1 = k \frac{1-\langle\alpha\rangle C_o}{\langle 1-\alpha\rangle} \tag{3-39}$$

$$C_2 = k\, C_o \tag{3-40}$$

$$\overline{C}_i = k^2\, C_i' \tag{3-41}$$

Eq. 3-38 takes the form

$$\frac{1}{A} f_i = \overline{C}_i \left| \frac{1-\langle\alpha\rangle C_o}{\langle 1-\alpha\rangle} \overline{V}_g - C_o \overline{V}_\ell \right| \left(\frac{1-\langle\alpha\rangle C_o}{\langle 1-\alpha\rangle} \overline{V}_g - C_o \overline{V}_\ell \right) = \Delta\rho g \langle(\alpha-\langle\alpha\rangle)^2\rangle \tag{3-42}$$

Eq. 3-42 can be rearranged to give

$$\overline{V}_g = C_o \langle j\rangle + \langle 1-\alpha\rangle \sqrt{\frac{\Delta\rho g}{\overline{C}_i} \langle(\alpha-\langle\alpha\rangle)^2\rangle} \tag{3-43}$$

$$\equiv C_o \langle j\rangle + \overline{V}_{gj} \tag{3-44}$$

This has been done by several authors (3,5), but it should be remembered that this is merely a convenient equation, and that in the above equations

$$C_o \neq \frac{\langle\alpha\, j\rangle}{\langle\alpha\rangle\langle j\rangle}$$

and

$$\overline{V}_{gj} \neq \frac{\langle\alpha\, V_{gj}\rangle}{\langle\alpha\rangle}$$

From the preceeding discussion, it can be seen that for both separated and dispersed flow the interfacial force can be modeled as

$$\overline{C}_i \left| \frac{1-\langle\alpha\rangle C_o}{\langle 1-\alpha\rangle} \overline{V}_g - C_o \overline{V}_\ell \right| \left(\frac{1-\langle\alpha\rangle C_o}{\langle 1-\alpha\rangle} \overline{V}_g - C_o \overline{V}_\ell \right)$$

Normally, the two-phase flow is neither fully dispersed nor fully separated, but a combination of both. Using Eqs. 3-19 and 3-20 we get

$$\overline{C}_i \frac{|\overline{V}_{gj}|\overline{V}_{gj}}{\langle 1-\alpha\rangle^2} = \Delta\rho g \langle\alpha\rangle \langle 1-\alpha\rangle \tag{3-45}$$

where

$$\overline{V}_{gj} = (1-\langle\alpha\rangle C_o)\,\overline{V}_g - \langle 1-\alpha\rangle\, C_o\, \overline{V}_\ell \tag{3-46}$$

With $\overline{V}_{gj}$ and C_o correlated from void fraction data, the interfacial friction factor can be correlated.

3.3 CORRELATION OF THE INTERFACE DRAG

In the previous two sections a methodology for the correlation of the interface drag based on void fraction data was developed. In this section, the methodology will be applied to specified flow regimes and a set of correlations for the interface drag for use in the BWR version of TRAC will be developed. The following flow regimes will be considered:

- Bubbly/Churn flow
- Annular flow
- Droplet flow

Furthermore, the combination of the latter two in the form of dispersed annular flow will also be considered as an intermediate state between the two idealized flow regimes.

3.3.1 Bubbly/Churn Flow

Combining Eqs. 3-21 and 3-45 gives

$$\frac{1}{8}\frac{\overline{C}_D}{d_i}\rho_c \frac{\overline{V}_{gj}^{\,2}}{\langle 1-\alpha\rangle^2} = \Delta\rho g \langle\alpha\rangle \langle 1-\alpha\rangle \tag{3-47}$$

For bubbly flow the liquid is the continuous phase, such that

$$\rho_c = \rho_\ell \tag{3-48}$$

Furthermore, the interface area can be given in terms of a critical Weber number

$$\frac{1}{d_i} = 6 \langle\alpha\rangle \frac{\rho_\ell \overline{V}_{gj}^{\,2}}{\sigma \, We_c \langle 1-\alpha\rangle^2} \tag{3-49}$$

Combining Eqs. 3-47, 3-48, and 3-49 gives

$$\frac{3}{4} \langle\alpha\rangle \frac{\overline{C}_D}{We_c} \frac{\rho_\ell^{\,2}}{\sigma} \frac{\overline{V}_{gj}^{\,4}}{\langle 1-\alpha\rangle^4} = \Delta\rho g \langle\alpha\rangle \langle 1-\alpha\rangle \tag{3-50}$$

Many expressions for $\overline{V}_{gj}$ have been reported in the literature (4,5,6), and many are of the form

$$\overline{V}_{gj} = k \left\{ \frac{\Delta\rho \; g \; \sigma}{\rho_\ell^{\,2}} \right\}^{0.25} \tag{3-51}$$

where k ranges from 1.18 to 1.53. A value for k of 1.41 is suggested by Ishii (3) and fits most data. Inserting Eq. 3-51 into Eq. 3-50 and using $k = 1.41 = \sqrt{2}$ results in

$$\frac{\overline{C}_D}{We_c} = \frac{1}{3} \langle 1-\alpha\rangle^5 \tag{3-52}$$

It is seen that the drag coefficient is proportional to the Weber number, but for the interfacial drag, We_c does not have to be specified. All we need to know is the ratio between $\overline{C}_D$ and We_c. The value of We_c will, however, have an influence on the interfacial heat transfer.

The distribution parameter will, for co-current flow, range from 0 for subcooled boiling to 1.333 as a maximum value for parabolic profiles. For high flow rates or high pressures ($\rho_g \approx \rho_\ell$), the distribution parameter should approach 1. Ishii recommends (3)

$$C_o = C_\infty - (C_\infty - 1) \sqrt{\frac{\rho_g}{\rho_\ell}} \tag{3-53}$$

where C_∞ is given by Nikuradse (7)

$$C_\infty = 1.393 - 0.015 \ln (Re) \tag{3-54}$$

3.3.2 Annular Flow

For annular flow the density of the liquid phase will be used in Eq. 3-47

$$\rho_c = \rho_\ell \tag{3-55}$$

and the interface area is given by*

$$\frac{1}{d_i} = \frac{4}{D_h} \sqrt{\alpha} \tag{3-56}$$

Combining Eqs. 3-47, 3-55, and 3-56 gives

$$\frac{1}{2} \sqrt{\alpha}\, \overline{C}_D \frac{\rho_\ell}{D_h} \frac{\overline{V}_{gj}^2}{\langle 1-\alpha \rangle^2} = \Delta\rho g \langle \alpha \rangle \langle 1-\alpha \rangle \tag{3-57}$$

Ishii (3) has analyzed the annular flow regime, using Wallis' (5) expression for the interface shear, and recommends

$$\overline{V}_{gj} = \frac{\langle 1-\alpha \rangle^{\frac{3}{2}}}{\langle \alpha \rangle + a} \sqrt{\frac{\Delta\rho g\, D_h}{0.0015\, \rho_\ell}} \tag{3-58}$$

Inserting Eq. 3-58 into Eq. 3-57 gives

$$\overline{C}_D = 0.03 \sqrt{\alpha}\ (\alpha + a)^2 \tag{3-59}$$

where

$$a = \sqrt{\frac{1 + 75 \langle 1-\alpha \rangle}{\sqrt{\alpha}} \frac{\rho_g}{\rho_\ell}}$$

*This equation holds only for a smooth film. For a rough film the interface area will be increased, however, we have chosen to include the effect of surface roughness into $\overline{C}_D$.

For the distribution parameter, Ishii recommends,

$$C_o = 1 + \frac{\langle 1-\alpha \rangle}{\alpha + a} \tag{3-60}$$

3.3.3 Droplet Flow

For droplet flow the continuous phase is the vapor phase

$$\rho_c = \rho_g \tag{3-61}$$

The interface area can be given in terms of a critical Weber number

$$\frac{1}{d_i} = 6 \langle 1-\alpha \rangle \frac{\rho_g \overline{V}_{gj}^2}{\sigma We_c \langle 1-\alpha \rangle^2} \tag{3-62}$$

Combining Eqs. 3-47, 3-61, and 3-62 results in

$$\frac{3}{4} \langle 1-\alpha \rangle \frac{\overline{C}_D}{We_c} \frac{\rho_g^2}{\sigma} \frac{\overline{V}_{gj}^4}{\langle 1-\alpha \rangle^4} = \Delta\rho g \langle \alpha \rangle \langle 1-\alpha \rangle \tag{3-63}$$

Many expressions for $\overline{V}_{gj}$ are reported in the literature (5), and many are of the form

$$\overline{V}_{gj} = k \langle 1-\alpha \rangle \left\{ \frac{\Delta\rho \, g \, \sigma}{\rho_g^2} \right\}^{\frac{1}{4}} \tag{3-64}$$

Ishii (3) recommends k = 1.41

Using Eq. 3-64 and k = 1.41 = $\sqrt{2}$ in Eq. 3-63 gives

$$\frac{\overline{C}_D}{We_c} = \frac{1}{3} \langle \alpha \rangle \tag{3-65}$$

As the droplets can be assumed uniformly distributed due to the turbulence, the distribution parameter is

$$C_o = 1 \tag{3-66}$$

For large flow rates where the droplets are created by entrainment from the film, the interface area per unit volume will be approximately

$$\frac{1}{d_i} = 1/2 \langle 1-\alpha \rangle \frac{\rho_g \langle j \rangle^2}{\sigma} \tag{3-67}$$

The droplets produced by the entrainment process can mainly be characterized as undistorted particles outside the Stokes regime (3). An approximation for the drag coefficient is

$$\bar{C}_D = 10.7 \alpha \, Re_d^{-1/2*} \tag{3-68}$$

An example of the prediction capability of the new shear model is given in Figures 3-2 through 3-4, where comparisons are made between TRAC calculations and CISE adiabatic tube data (8).

The main data for the tests are given in Table 3-1. The agreement between the calculation and the data is generally seen to be excellent. In Figure 3-4, however, void fraction over 80% is slightly overpredicted. This is most likely due to an overprediction of the entrainment for the very large flow rate in this test.

Table 3-1

MAIN DATA FOR CISE ADIABATIC TESTS

	Case 1	Case 2	Case 3
Test section	Vertical	Vertical	Vertical
Length, in	4.14	4.14	4.14
Inner diameter, mm	9.1	9.1	9.1
Pressure, MPa	2.932	4.923	4.894
Flow rate, kg/m^2s	1081	388	2143
Inlet subcooling, °K	0	0	0
Inlet quality, %	0-75	0-80	0-41

*Combining Eqs. 3-47, 3-61, 3-67, and 3-68 gives,

$$V_{gj} = \frac{\langle 1-\alpha \rangle^2}{0.67} d_i \left[\frac{(\Delta\rho \, g)^2}{\mu_g \, \rho_g} \right]^{(1/3)}$$

which is in agreement with the expression recommended by Ishii (3).

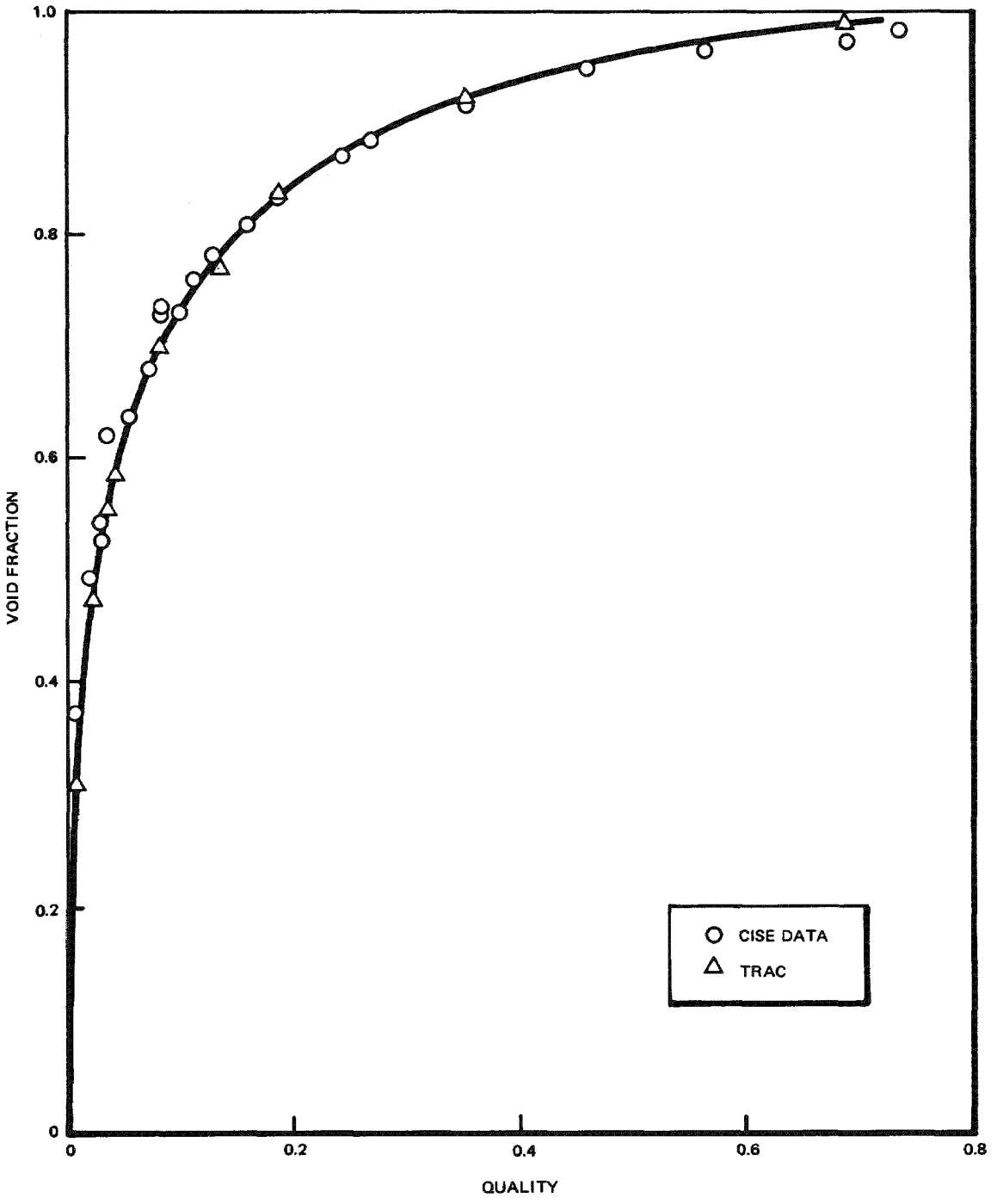

Figure 3-2. Case 1, CISE Tube Data: P = 2.932 MPa, G = 1081 kg/m^{2}s

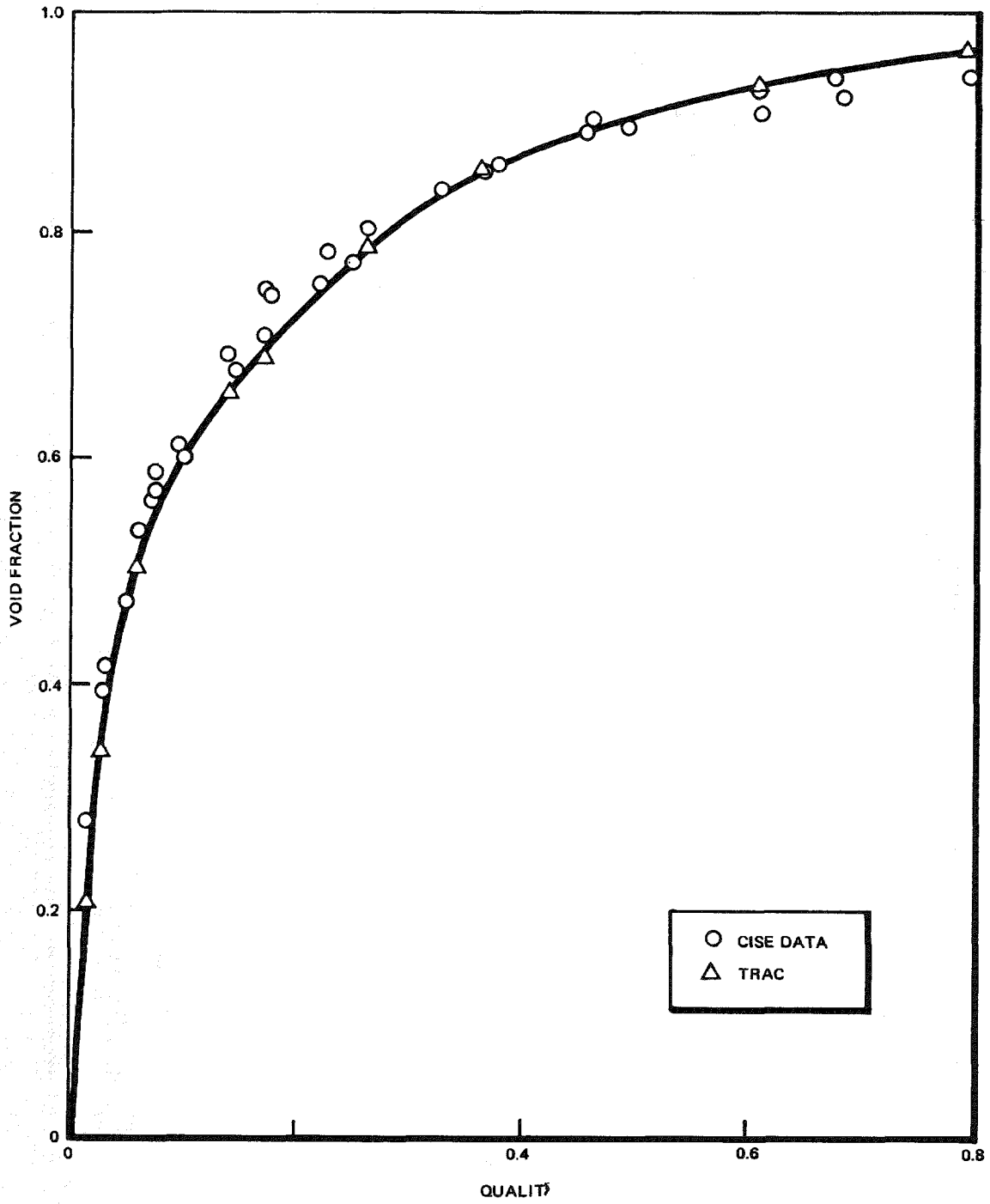

Figure 3-3. Case 2, CISE Tube Data: P = 4.923 MPa, G = 388 kg/m^{2}s

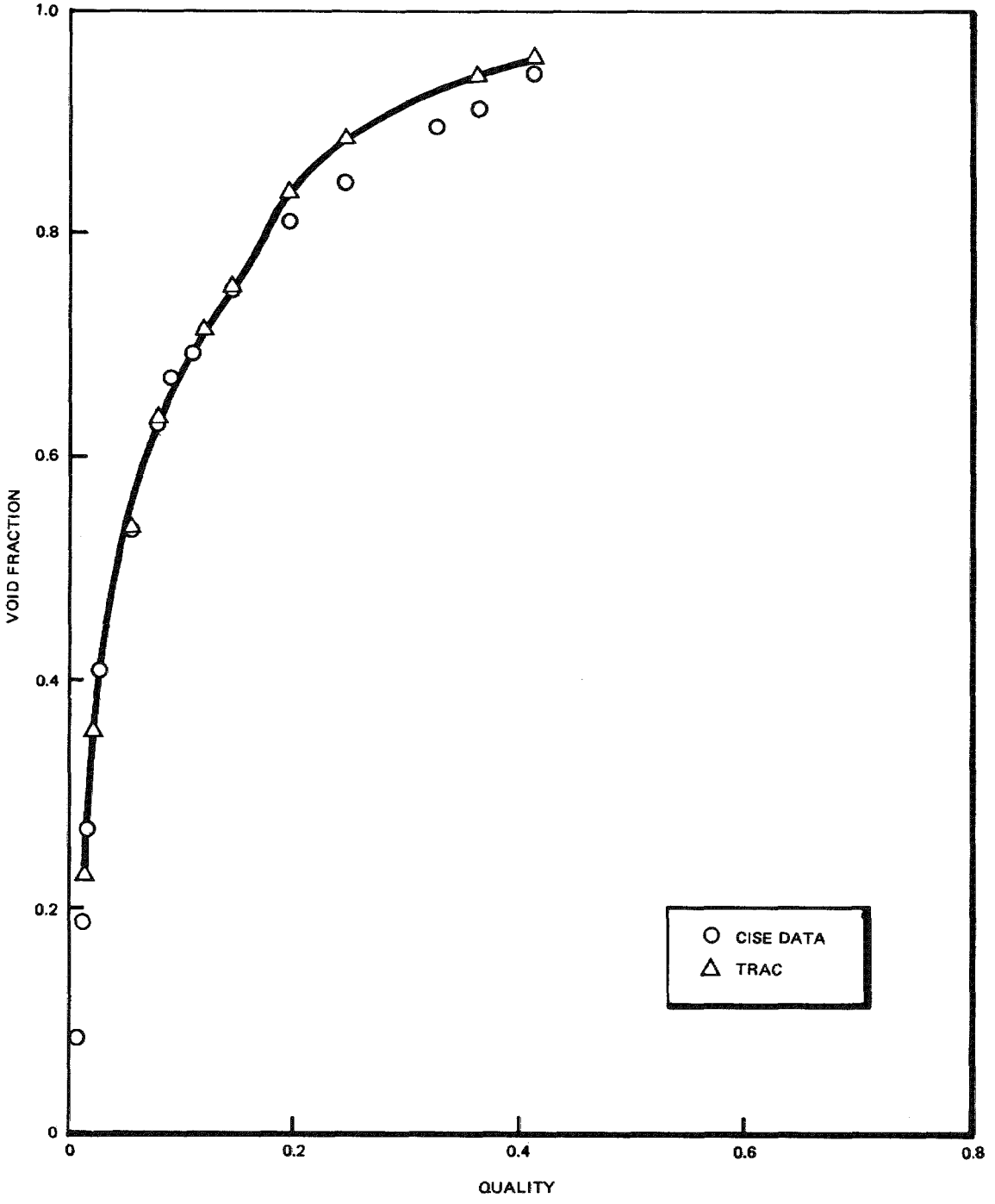

Figure 3-4. Case 3, CISE Tube Data: P = 4.894 MPa, G = 2143 kg/m^{2}s

3.4 FLOW REGIME TRANSITIONS

With the flow regimes described in Section 3.3, two transitions need to be considered:

- The transition between bubbly/churn flow and annular flow
- The onset of entrainment

The transition between bubbly/churn flow and annular flow has been widely analyzed (3). The criterion for transition is when the liquid in the film (or entrained droplets) can be lifted by the vapor flow (3,9). This, however, is only true for the case when $j_\ell = 0$; for cocurrent upflow the criterion should be modified so that transition takes place when the liquid in the film (or entrained droplets) can be lifted relative to liquid velocity in the bubbly churn flow regime. With this modification the transition is given by the intercept between the two flow correlations.

The transition between annular flow and dispersed annular flow is given by the onset of entrainment. The correlation proposed by Ishii (10, 11) has been adopted.

In TRAC-B01, however the entrainment is calculated by a modified version of Ishii's entrainment correlation (11). The correlation is

$$E = \frac{\eta}{\sqrt{1 + (\eta + 0.1)^2}} \tag{3-69}$$

where

$$\eta = 8.0 \times 10^{-7} \; j_g^{*2.5} \; D^{*1.25} \; Re^{0.25} \tag{3-70}$$

in which

$$j_g^* = \frac{j_g}{\left[\frac{\sigma \, \Delta\rho \, g}{\rho_g^2}\left(\frac{\rho_g}{\Delta\rho}\right)^{0.667}\right]^{0.25}} \tag{3-71}$$

$$Re = \frac{\rho_\ell \, j_\ell \, D}{\mu_\ell} \tag{3-72}$$

$$D^* = D \sqrt{\frac{g\Delta\rho}{\sigma}} \tag{3-73}$$

Ishii's original correlation was E = const x tgh (0.9 η); however, the asymptotic behavior of tgh(η) for large η leads to an overprediction of α for large flow rates. Ishii (11) and Ishii and Grolmes (10) have shown that the entrainment for large flow rates is given by $E = 1 - \text{const}/j_g^3$, and Eq. 3-69 is in better agreement with this asymptotic behavior.

For dispersed annular flow $\bar{V}_{gj}$ as shown by Ishii (3) is then given by

$$\bar{V}_{gj} = \frac{\langle 1-\alpha\rangle (1-E)}{\alpha + \sqrt{\frac{1 + 75 \langle 1-\alpha\rangle}{\sqrt{\langle\alpha\rangle}} \frac{\rho_g}{\rho_\ell}}} \sqrt{\frac{\Delta\rho \, g \, D \langle 1-\alpha\rangle (1-E)}{0.015 \, \rho_\ell}}$$

$$+ \frac{E \langle 1-\alpha\rangle}{\langle\alpha\rangle + E \langle 1-\alpha\rangle} \begin{cases} \sqrt{2} \left(\frac{\Delta\rho \, g \, \sigma}{\rho_g^2}\right)^{0.25} \\ \frac{3\sigma}{\rho_g} \left(\frac{(\Delta\rho \, g)^2}{\mu_g \, \rho_g}\right)^{1/3} \end{cases} \quad \frac{1}{\langle j\rangle^2} \quad \text{for large (j)} \tag{3-74}$$

and C_o is given by

$$C_o = 1 + \frac{\langle 1-\alpha\rangle (1-E)}{\langle\alpha\rangle + \sqrt{\frac{1 + 75 \langle 1-\alpha\rangle}{\sqrt{\langle\alpha\rangle}} \frac{\rho_g}{\rho_\ell}}} \tag{3-75}$$

It should be noted that Eq. 3-69 applies primarily for cocurrent annular flow and that further research and development on entrainment and deposition is recommended.

3.5 COUNTER CURRENT FLOW

Very few data for the void fraction exist for counter current flow; however, a large data base for counter-current flow limitation (CCFL) exists. From Eq. 3-33 and 3-35

$$\langle j_g \rangle = \frac{\langle \alpha \rangle C_o}{1 - \langle \alpha \rangle C_o} \langle j_\ell \rangle + \frac{\langle \alpha \rangle}{1 - \langle \alpha \rangle C_o} \bar{V}_{gj} \tag{3-76}$$

The general form for CCFL correlations is given by

$$\sqrt{\frac{\langle j_g \rangle}{j_{go}}} + \sqrt{\frac{\langle j_\ell \rangle}{j_{\ell o}}} = 1 \tag{3-77}$$

where j_{go} and $j_{\ell o}$ represent the intercept with the axis. Because the drift flux correlation should describe all possible flow situations at or below the CCFL curve (see Figure 3-5), the line given by Eq. 3-76 for constant (α) should be tangent to the CCFL curve.

This puts a constraint on C_o and $\bar{V}_{gj}$. By requiring that Eq. 3-76 be tangent to Eq. 3-77, we get

$$\frac{\bar{V}_{gj}}{-j_{\ell o}} = \frac{C_o (1 - \langle \alpha \rangle C_o)}{-\frac{j_{\ell o}}{j_{go}} \langle \alpha \rangle C_o + 1 - \langle \alpha \rangle C_o} \tag{3-78}$$

The CCFL correlation that will be used is given by the Kutateladze numbers,

$$\sqrt{K_g} + m\sqrt{-K_\ell} = \sqrt{K} \tag{3-79}$$

where

$$K_g = \frac{\langle j_g \rangle \sqrt{\rho_g}}{(\Delta\rho\, g\, \sigma)^{0.25}} \tag{3-80}$$

$$K_\ell = \frac{\langle j_\ell \rangle \sqrt{\rho_\ell}}{(\Delta\rho\, g\, \sigma)^{0.25}} \tag{3-81}$$

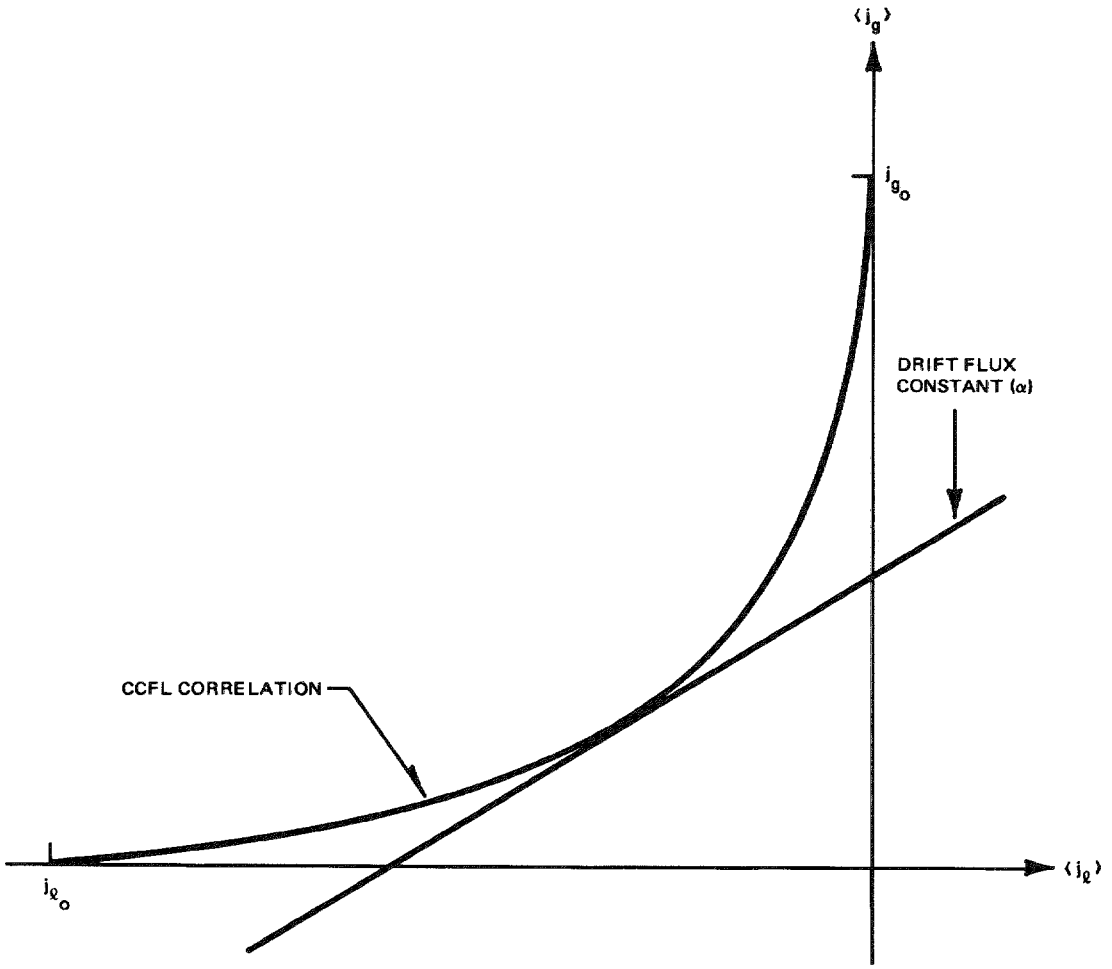

Figure 3-5. Drift Flux Correlation and CCFL

For counter-current flow, C_o is not very well defined; e.g., for dispersed flow, C_o has a singularity for $\langle j \rangle = 0$. Consequently, $\overline{V}_{gj}$ will be determined as described in Section 3.3 and C_o will be determined from Eq. 3-78.

Counter-current flow is a flow regime where the details of the flow are not well understood and where further development will be made, as more data and better understanding become available.

A comparison between TRAC and CCFL data (12) is shown in Figure 3-6. The main data for the test is given in Table 3-2. The data are for subcooled liquid and show CCFL breakdown occurs when all the steam can be condensed by the subcooled liquid. It is seen that TRAC is within the variance of the data, where CCFL exist, and that the subcooled CCFL breakdown is well predicted.

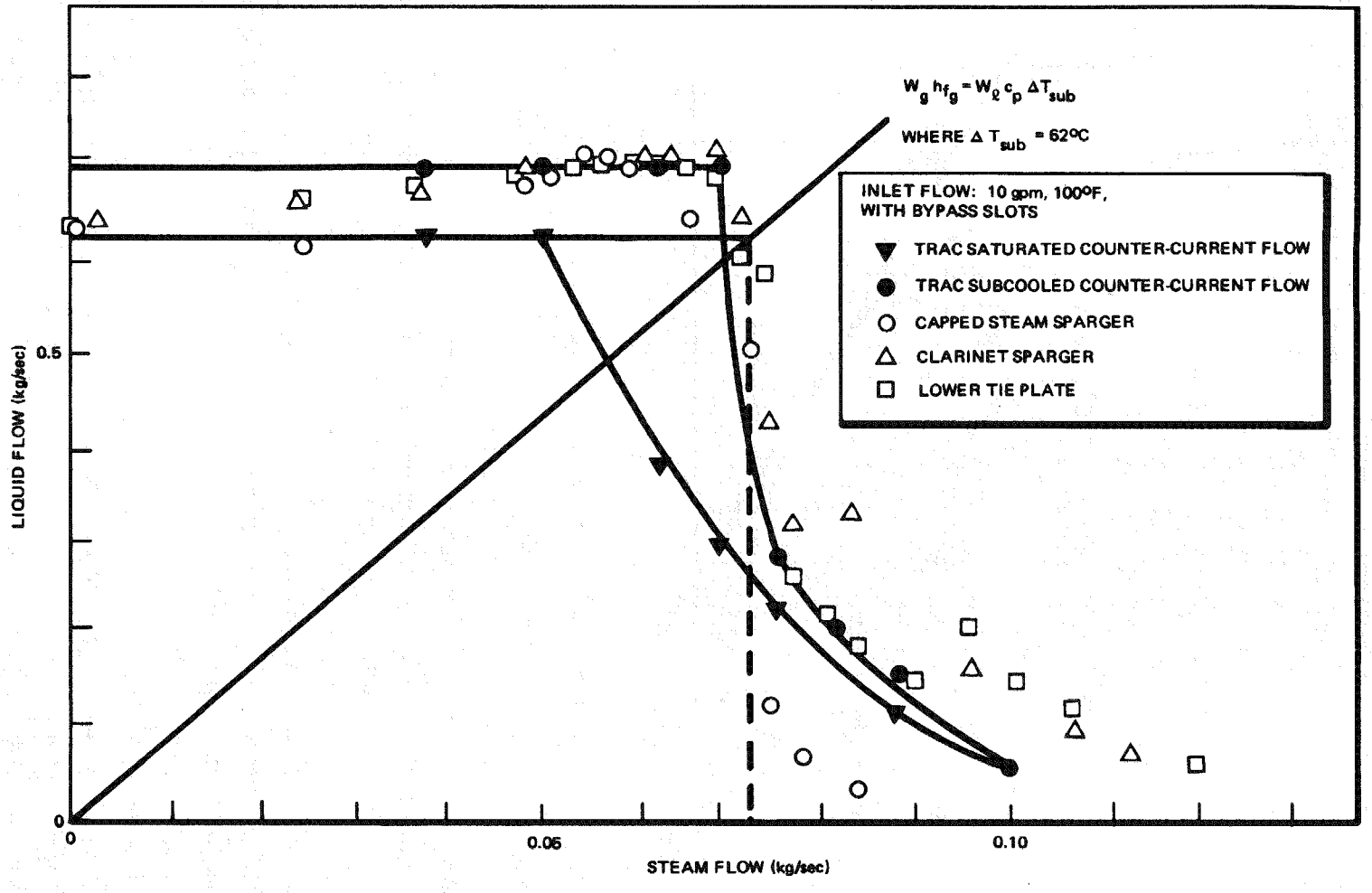

Figure 3-6. Effect of Steam Injection

Table 3-2

MAIN DATA FOR CCFL TESTS

Pressure	0.1013 MPa
Liquid flow	0.6305 kg/s
Liquid subcooling	62°K
Steam flow	0.03736 to 0.09962 kg/s
Upper tie plate flow area	7.674×10^{-3} m^2

3.6 VIRTUAL MASS

The virtual mass is normally a small term, compared to the other term in the momentum equation. Only for critical flow or sudden accelerations due to abrupt area changes is it of importance. The inclusion of the virtual mass was also found to have a positive effect on the stability of the numerical method used for the integration of the conservation equations. This was found to be particularly important for counter-current flow.

The virtual mass (see Eqs. 2-3 and 2-4) is given by

$$k = 1 \tag{3-82}$$

$$\rho_c = (\langle 1-\alpha \rangle \sqrt{\rho_\ell} + \langle \alpha \rangle \sqrt{\rho_g})^2 \tag{3-83}$$

$$\bar{V}_{di} = \langle 1-\alpha \rangle \bar{V}_g + \langle \alpha \rangle \bar{V}_\ell \tag{3-84}$$

For a single spherical particle in an infinite medium, k = 0.5; for closely packed bubbles, k may be in the range of 2 to 3; a value of k = 1 has been chosen as an average value. For C_o = 1 and m = 1, Eqs. 3-78, 3-79, 3-80, and 3-81 reduce to

$$V_{gj} = \langle 1-\alpha \rangle \frac{K\,(\Delta\rho\, g\, \sigma)^{0.25}}{\langle 1-\alpha \rangle \sqrt{\rho_\ell} + \langle \alpha \rangle \rho_g}$$

Comparing this expression to the bubble size velocity (Eq. 3-51) and the free fall velocity for a droplet (Eq. 3-64), it is seen that $(\langle 1-\alpha \rangle \sqrt{\rho_\ell} + \langle \alpha \rangle \sqrt{\rho_g})^2$ represents the density of the continuous phase in both limits. For this reason the

above expression was chosen for the density of the continuous phase. The expression for the velocity of the dispersed phase was chosen to have the right limits.

3.7 3-DIMENSIONAL FLOW CONSIDERATIONS

For 3-dimensional flow the calculation of the interfacial shear is based on the assumption that correlations for the interface drag or shear for a given flow regime are applicable independent of the direction of the flow. This assumption is justified, because for a given flow regime the interface shear and drag should be given only by the phase velocities and the phase and velocity distributions. However, the body force, i.e., the gravity, only acts in the vertical direction, and thus for horizontal flow, only the phase and velocity profiles will produce a net relative velocity between the phases.

Section 4
HEAT TRANSFER

The heat transfer analysis in the TRAC code can be divided into two essentially separate sections: the heat transfer at the wall and the liquid-vapor interface. The wall heat transfer, specified by the appropriate constitutive correlations, couples the heat conduction equation for the wall and the energy equations for the two-phase mixture, while the interfacial heat transfer couples the energy and mass balance equations of liquid and vapor. Since correlations for transient conditions are scarce, steady-state correlations are used to calculate the heat transfer based on local conditions. However, the steady-state correlations were found to be adequate in most cases.

After reviewing the heat transfer correlations used in TRAC-P1A(1), several areas were either added or modified for improvement. Subcooled boiling and thermal radiation were added to the heat transfer package. The boiling transition correlation used by the fuel bundle is changed from the Biasi correlation to the CISE-GE correlation. These are the major differences in the heat transfer correlations between the current TRAC code and the TRAC-P1A code. The following sections describe the heat transfer correlations to be used in the BWR version of TRAC. New models or changes are denoted by an asterisk.

For the present, the interfacial areas for heat transfer as used in TRAC-P1A have been retained. In the future, consideration will be given to obtaining one consistent set of interfacial areas for heat and momentum transfer.

4.1 WALL HEAT TRANSFER

The heat transfer coefficients used in the BWR version of TRAC are obtained from a boiling curve (see Figure 4-1) constructed for the given set of fluid and wall conditions. The heat transfer coefficient correlations used in constructing this curve are coded in a subroutine named HTCØR and in a series of subroutines called by HTCØR. This package of subroutines is used for all conditions and in all components where the heat transfer coefficients are required. For a given set of conditions (i.e., α, v_ℓ, v_g, T_w, T_ℓ, T_g, and T_s), the heat transfer coefficient is found in the manner illustrated in the flow diagram of subroutine HTCØR (Figure 4-2).

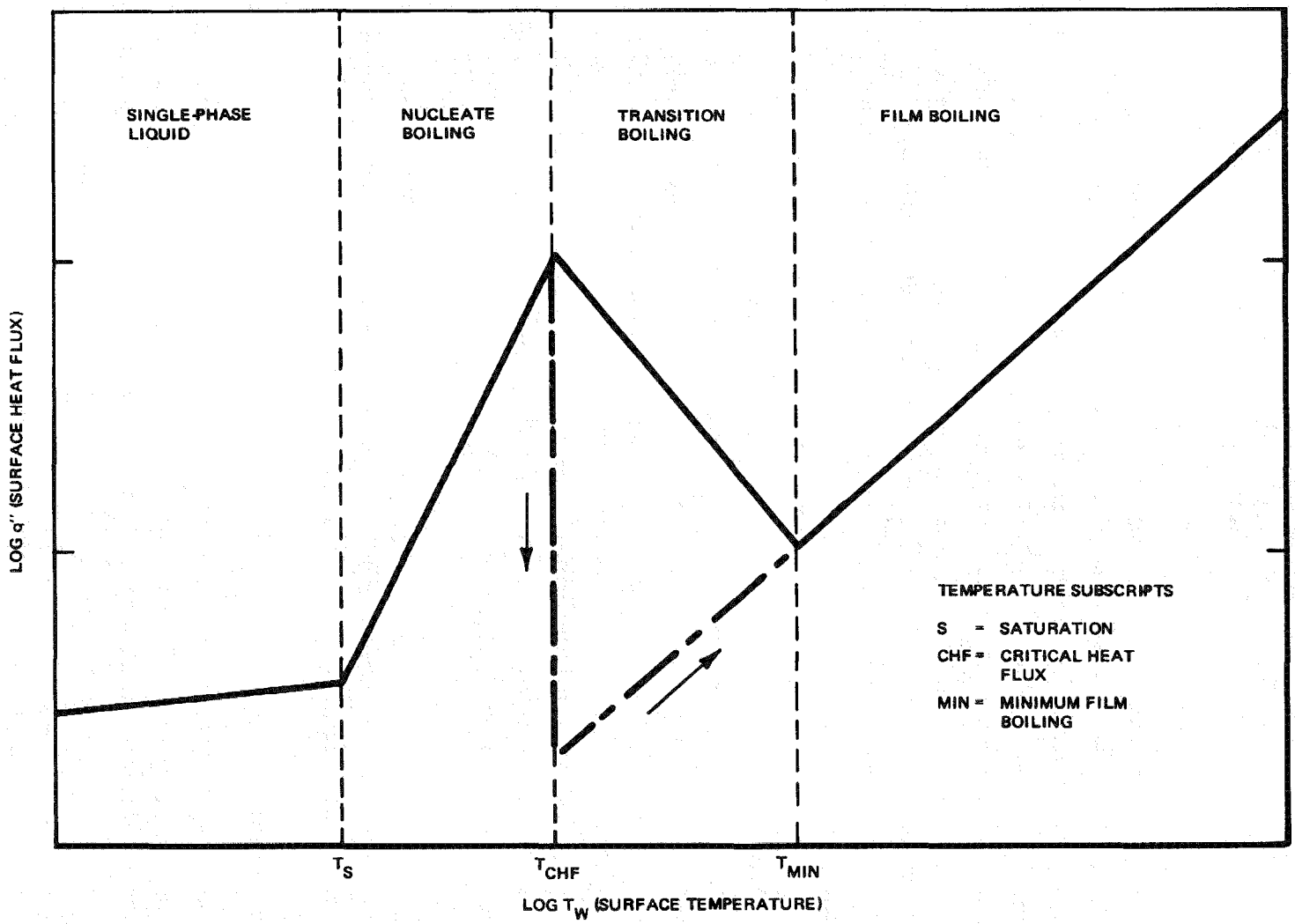

Figure 4-1. Generalized Boiling Curve

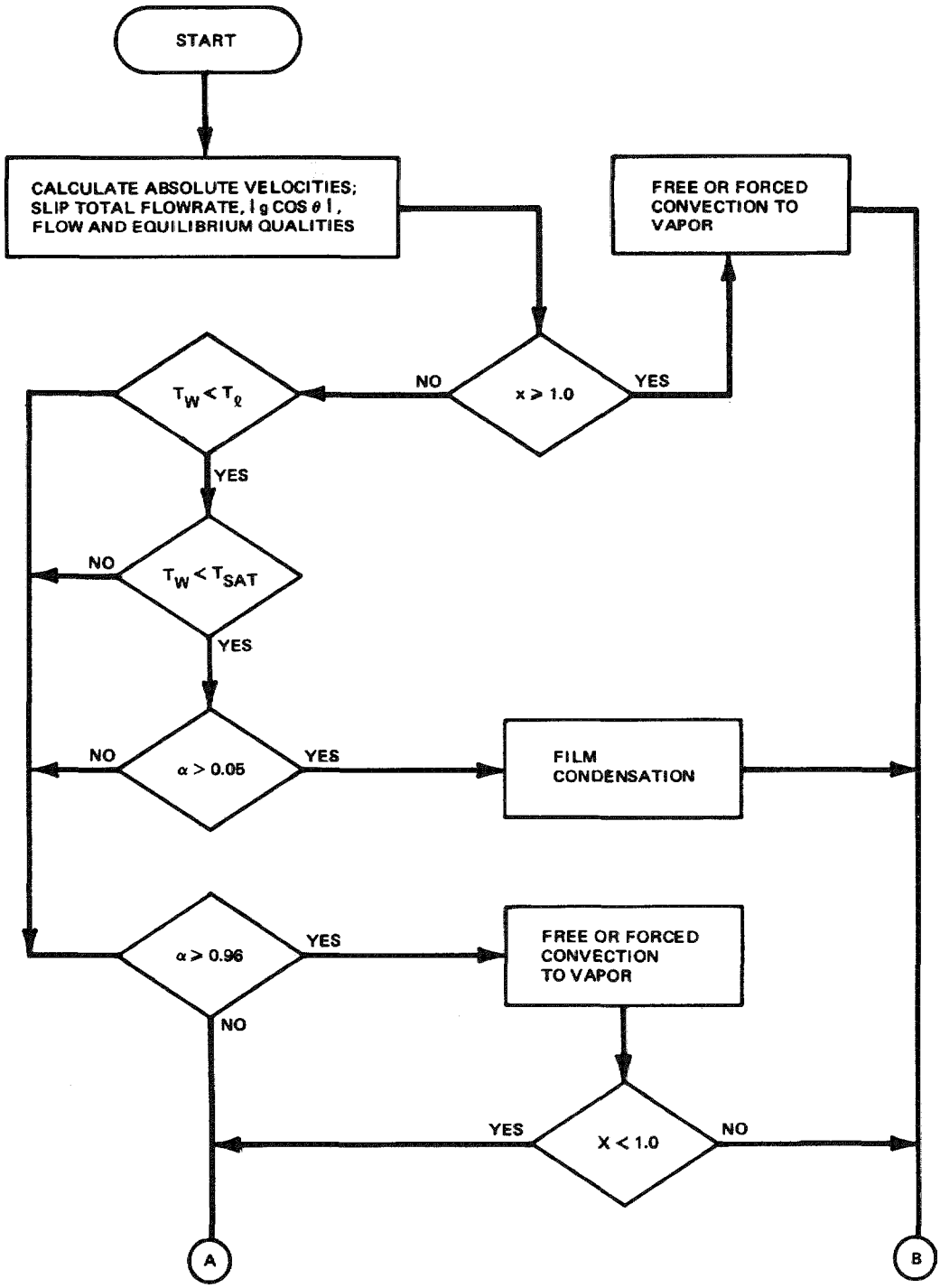

Figure 4-2. Flowchart for HTCØR

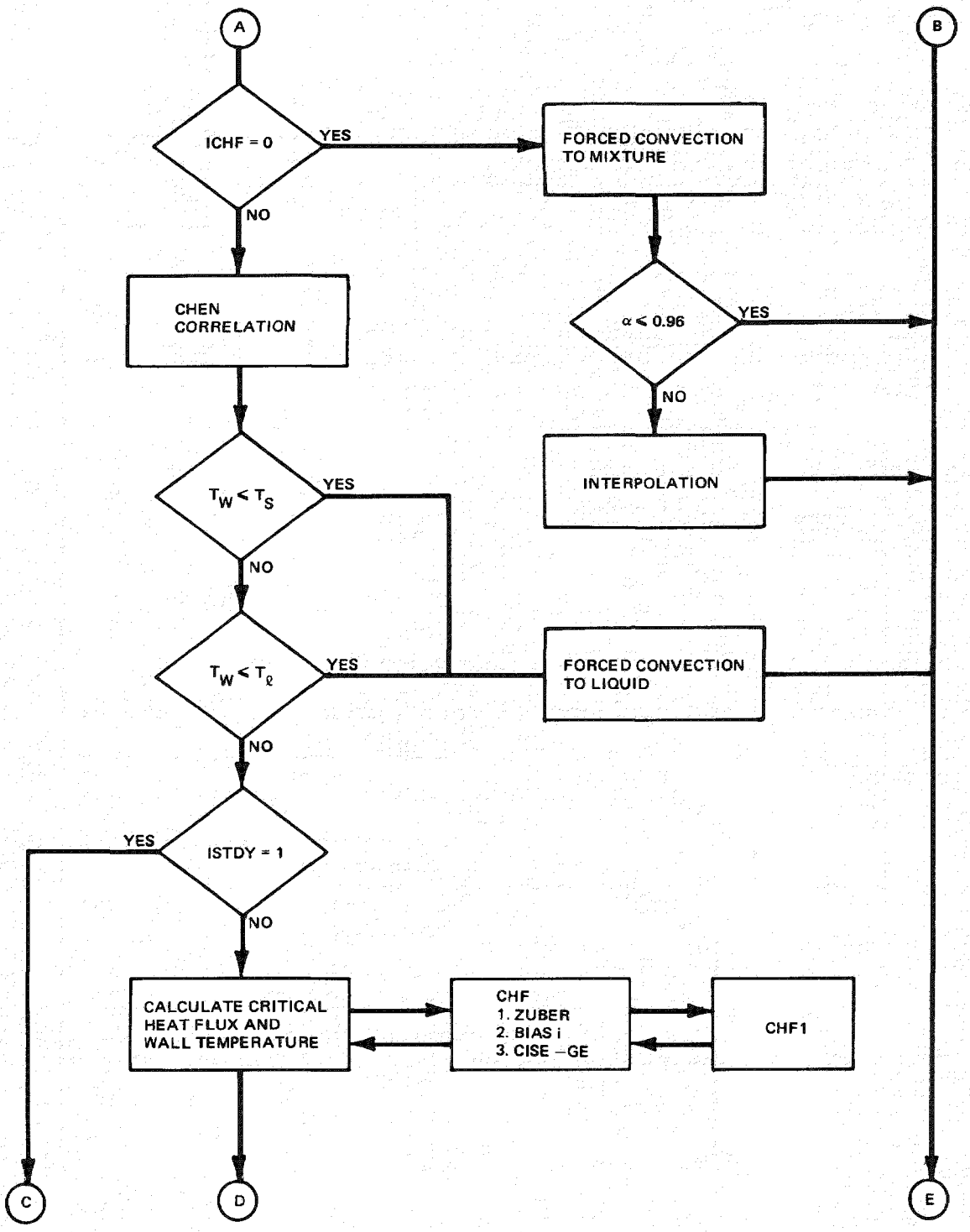

Figure 4-2. Flowchart for HTCØR (Continued)

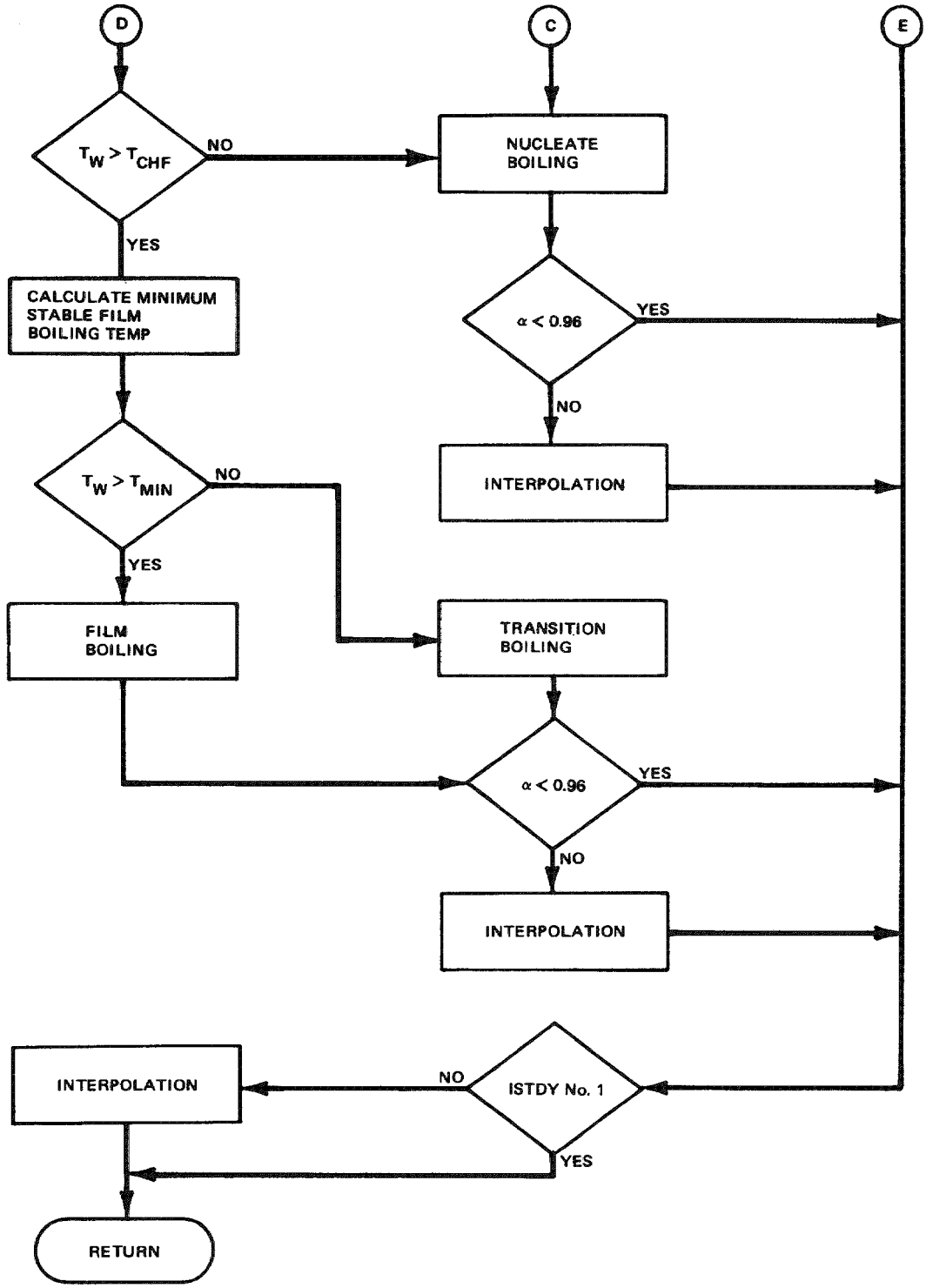

Figure 4-2. Flowchart for HTCØR (Continued)

4.1.1 Heat Transfer Coefficient Correlations

4.1.1.1 Regime 1 - Forced and Free Convection to Single Phase Liquid. The heat transfer coefficients in this regime are given as follows:

$$h_g = 0 \tag{4-1}$$

and

$$h_\ell = \begin{cases} h_{FORC}, & \text{If } \overline{Re}_\ell \neq 0 \text{ and } Gr/\overline{Re_\ell}^2 \leq 1.0 \\ h_{FREE} \end{cases} \tag{4-2}$$

where

$$h_{FORC} = \max \left\{ h_{lam}, h_{turb} \right\} \tag{4-3}$$

in which

$$h_{lam}(13) = 4k_\ell / D_h \tag{4-4}$$

$$h_{turb}(14) = 0.023 \frac{k_\ell}{D_h} \left[\frac{G(1-x)\, D_h}{\mu_\ell} \right]^{0.8} \left[\frac{\mu_\ell C_{p,\ell}}{k_\ell} \right]^{0.4} \tag{4-5}$$

$$\overline{Re}_\ell = \overline{\rho_\ell} \nu_{\ell z} D_h / \mu_\ell \tag{4-6}$$

$$Gr_\ell = g_c \beta \left| T_w - T_\ell \right| \bar{\rho}^2 D_h^3 / \mu_\ell^2 \tag{4-7}$$

$$\overline{\rho}_\ell = \rho_\ell + \frac{\partial \rho_\ell}{\partial T_\ell} (T_{film} - T_\ell) \tag{4-8}$$

$$T_{film} = \frac{1}{2} (T_w + T_\ell) \tag{4-9}$$

$$\beta = -\frac{\partial \rho_\ell}{\partial T_\ell} \Big/ \bar{\rho}_\ell \tag{4-10}$$

$$h_{FREE}(15) = \begin{cases} (k_\ell/D_h)(0.59)(Gr_\ell Pr_\ell)^{0.25} & \text{if } Gr_\ell Pr_\ell \leq 10^9 \\ (k_\ell/D_h)(0.1)(Gr_\ell Pr_\ell)^{0.333} & \end{cases} \tag{4-11}$$

in which

$$Pr_\ell = \frac{\mu_\ell C_{p,\ell}}{k_\ell} \tag{4-12}$$

4.1.1.2 Regime 2 - Nucleate Boiling. The heat transfer coefficients in this regime are given as follows:

$$h_g = 0 \tag{4-13}$$

and

$$h = h_{CHEN}(16) \tag{4-14}$$

where

$$h_{CHEN} = F\, h_{FORC} + F_s\, h_{NUCL} \tag{4-15}$$

in which

F = Reynolds number factor defined in page 54 of the TRAC P1A manual (1)

h_{FORC} = Single phase liquid forced convection heat transfer coefficient defined in regime 1

F_s = Subcooled correction factor

$$= \begin{cases} 1 & \text{if } T_\ell \geq T_s \\ (T_w - T_s)/T_w - T_\ell) & \text{if } T_\ell < T_s \end{cases} \tag{4-16}$$

$$h_{NUCL} = 0.00122$$

$$= \frac{k_\ell^{0.79}\, C_{p,\ell}^{0.45}\, \rho_\ell^{0.49}}{\sigma^{0.5}\, \mu_\ell^{0.29}\, h_{fg}^{0.24}\, \rho_g^{0.24}} (\Delta T)^{0.24}\, (\Delta\rho)^{0.75}\, S \qquad (4\text{-}17)$$

and

$$\Delta T = T_w - T_s \qquad (4\text{-}18)$$

$$\Delta P = P_s - P \qquad (4\text{-}19)$$

P_s = Saturation pressure corresponding to T_w

S = Suppression factor defined in page 54 of the TRAC P1A manual (1)

4.1.1.3 Regime 3 - Transition Boiling. The heat transfer coefficients in this regime are given as follows:

$$*h_g = (1-\gamma)\, h_{g,min} (T_{min} - T_g)/T_w - T_g) \qquad (4\text{-}20)$$

and

$$*h_\ell = \frac{[\gamma h_{\ell,CHF}\, (T_{CHF} - T_\ell) + (1-\gamma)\, h_{\ell,min}\, (T_{min} - T_\ell)]}{T_w - T_\ell} \qquad (4\text{-}21)$$

where

$$\gamma = \left(\frac{T_w - T_{min}}{T_{CHF} - T_{min}}\right)^2 \qquad (4\text{-}22)$$

and

T_{min} = Minimum stable film boiling temperature

T_{CHF} = Temperature at critical heat flux

*New models or changes

$h_{g,min}$ = Vapor heat transfer coefficient in film boiling regime evaluated at T_{min}

$h_{\ell,min}$ = Liquid heat transfer coefficient in film boiling regime evaluated at T_{min}

$h_{\ell,CHF}$ = Liquid heat transfer coefficient in nucleate boiling regime evaluated at T_{CHF}

$= h_{CHEN}\ (T_{CHF})$

4.1.1.4 Regime 4 - Film Boiling. The liquid and vapor heat transfer coefficients in this regime are given as follows:

$$h_{\ell} = (1-\alpha)\ \frac{T_w - T_s}{T_w - T_{\ell}}\ h_R \tag{4-23}$$

and

$$h_g = (1-\alpha)\ h_B + \alpha \max\ \{h_{g,NC},\ h_{g,DR}\} \tag{4-24}$$

where

h_R = HTC for radiation between wall and liquid

$$= \sigma\varepsilon\left(T_w^4 - T_s^4\right)\Big/\left(T_w - T_s\right) \tag{4-25}$$

σ = Stefan-Boltzman constant

ε = Wall emissivity

$h_{g,NC}$ = Heat transfer coefficient for vapor natural convection (will be discussed in Regime 6)

$h_{g,DR}$(17) = Dougall-Rohsenow Correlation

$$= 0.023\ \frac{k_g}{D_h}\left[\frac{\rho_g[\alpha v_g + (1-\alpha)v_{\ell}]\ D_h}{\mu_g}\right]^{0.8}\left(\frac{C_{p,g}\mu_g}{k_g}\right)^{0.4} \tag{4-26}$$

h_B(18) = Bromley Correlation

$$= 0.62 \left[\frac{k_g^3 (\rho_\ell - \rho_g)\, g h'_{fg} \rho_g}{\mu_g (T_w - T_s) \lambda} \right]^{0.25} \tag{4-27}$$

in which

$$h'_{fg} = h_{fg} + 0.5\, C_{p,g} (T_g - T_s) \tag{4-28}$$

$$\lambda = 2\pi \left[\frac{\sigma}{g(\rho_\ell - \rho_g)} \right]^{1/2} \tag{4-29}$$

α = Void fraction

4.1.1.5 Regime 6 - Forced or Natural Convection to Vapor. The heat transfer coefficients in this regime are given as follows:

$$h_\ell = 0 \tag{4-30}$$

and

$$h_g = \max \{h_{g,NC}, h_{g,turb}\} \tag{4-31}$$

where

$h_{g,NC}$(19) = McAdam Correlation for natural convection

$$= 0.13 \frac{k_g}{D_h} \left[\frac{D_h^3 \rho_g^2 g \left| T_w - T_g \right|}{\mu_g^2 T_g} \right]^{1/3} \left(\frac{C_{p,g} \mu_g}{k_g} \right)^{1/3} \tag{4-32}$$

$$h_{g,turb}(14) = 0.023 \frac{k_g}{D_h} \left(\frac{\rho_g v_g D_h}{\mu_g} \right)^{0.8} \left(\frac{C_{p,g} \mu_g}{k_g} \right)^{0.3} \tag{4-33}$$

4.1.1.6 Regime 7 - Forced Convection to Mixture. When the critical heat flux calculation is not asked for by the user (ICHF = 0), the heat transfer coefficient is calculated in the following manner:

$$h_g = \max \{h_{g,NC}, h_{g,turb}\} \tag{4-34}$$

and

$$h_\ell = \max \{h_{lam}, h_{turb}\} \tag{4-35}$$

where

$h_{g,NC}$(19) = McAdams Correlation (see Eq. 4-32)

$$h_{g,turb}(14) = 0.023 \frac{k_g}{D_h} \left(\frac{\rho_g v_g D_h}{\mu_g} \right)^{0.8} Pr_\ell^{1/3} \tag{4-36}$$

$$h_\ell(13) = 4\ k_\ell / D_h \tag{4-37}$$

$$h_{\ell,turb} = 0.023 \frac{k_\ell}{D_h} Re_m^{0.8} Pr_\ell^{0.4} \tag{4-38}$$

in which

$$Re_m = GD_h/\mu_m \tag{4-39}$$

and

$$\mu_m^{-1} = X_{flow}\, \mu_g^{-1} + (1-X_{flow})\, \mu_\ell^{-1} \tag{4-40}$$

and

X_{flow} = Flow Quality

4.1.1.7 Regimes 11, 12, and 13 - Condensation. The heat transfer coefficients in these regimes are given as follows:

$$h_g = 0 \tag{4-41}$$

and

$$h_\ell = \max \{h_{c,turb}, h_{c,lam}\} \tag{4-42}$$

where

$h_{c,turb}$(20) = Heat transfer coefficient for turbulent film condensation (regime 13)

= Carpenter and Colburn correlation

$$= 0.065 \left(\frac{\rho_\ell k_\ell C_{p,\ell}}{\mu_\ell}\right)^{1/2} \tau^{1/2} \tag{4-43}$$

in which

$$\tau^{1/2} = 0.046 \left[\left(\frac{G_g D_h}{\mu_g}\right)^2 \left(\frac{\rho_g v_g^2}{2}\right)\right] \tag{4-44}$$

$h_{c,lam}$ = Heat transfer coefficient for laminar film condensation

$$= \begin{cases} \text{Horizontal film condensation if } |g \cos\theta| \leq 0.5 \\ \text{Vertical film condensation if } |g \cos\theta| > 0.5 \end{cases}$$

$$= \begin{cases} 0.296 \left\{\dfrac{\rho_\ell(\rho_\ell-\rho_g)\, g\, h_{fg}\, k_\ell^3}{D_h \mu_\ell |T_w - T_s|}\right\}^{1/4} & \text{(Regime 11)} \quad (4\text{-}45) \\ 1.132 \left\{\dfrac{\rho_\ell(\rho_\ell\ \rho_g)\, g\, h_{fg}\, k_\ell^3}{D_h \mu_\ell |T_w - T_s|}\right\}^{1/4} & \text{(Regime 12)} \quad (4\text{-}46) \end{cases}$$

in which

θ = Angle between the axis of the cell and the vertical.

The horizontal laminar condensation heat transfer coefficient is obtained from Chato (21), while the vertical laminar condensation heat transfer coefficient is obtained by multiplying the original Nusselt formulation by 1.2 (22) to account for the waviness of the film.

4.1.2 Boiling Transition Criteria

The modified Zuber correlations and the Biasi correlation shown in the following are used to determine the critical heat flux under different flow conditions according to the schematic flow chart shown in Figure 4-3.

Zuber Correlation (23)

$$q_{CHF} = (1-\alpha)\left\{(0.9)(0.131)\,\rho_g h_{fg}\left[\frac{\sigma g(\rho_\ell - \rho_g)}{\rho_g^2}\right]^{1/4}\right.$$

$$+ F_s(0.696)\sqrt{\rho_\ell C_{p\ell} k_\ell}\left[\frac{g(\rho_\ell - \rho_g)}{\sigma}\right]^{1/4}\left[\frac{\sigma g(\rho_\ell - \rho_g)}{\rho_g^2}\right]^{1/8}$$

$$\left.\left(T_s - T_\ell\right)\right\} \qquad (4\text{-}47)$$

where

F_s = Subcooled correction factor

$$= \begin{cases} 1 \text{ if } T_{sat} > T \\ 0 \text{ - otherwise} \end{cases} \qquad (4\text{-}48)$$

Biasi Correlation (24)

$$q_{CHF} = \{q_1, q_2\} \qquad (4\text{-}49)$$

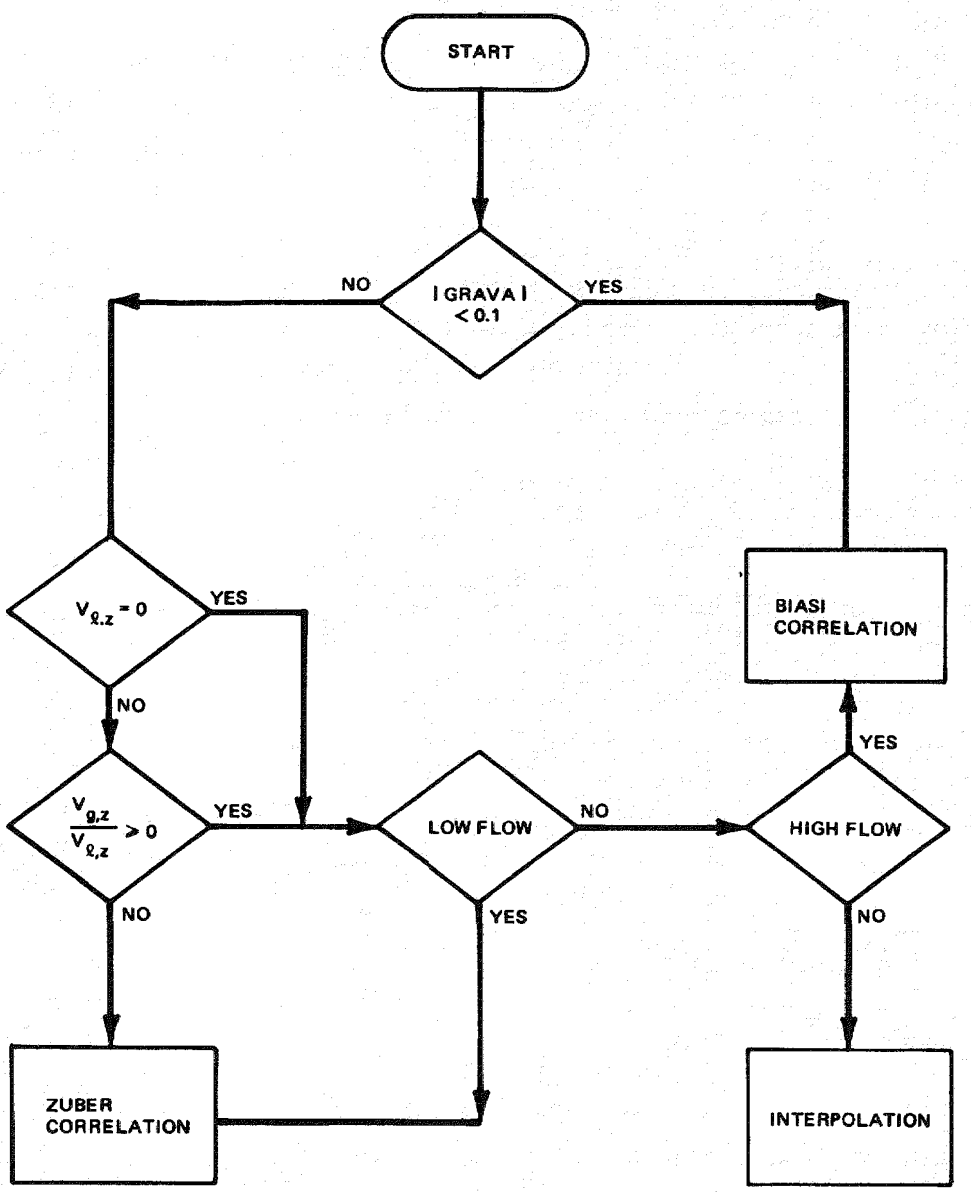

LOW FLOW: $-600 \leq G \leq 100$ kg/m^2

HIGH FLOW: $G > 200$ kg/m^2; $G < -700$ kg/m^2

GRAVA = $\cos\theta$

Figure 4-3. Flow Chart for CHF

$$q_1 = \frac{3.78 \times 10^7}{(100D)^n \left(\frac{G}{10}\right)^{0.6}} h_p(1-X) \tag{4-50}$$

$$q_2 = \frac{1.883 \times 10^7}{(100D)^n \left(\frac{G}{10}\right)^{1/6}} - \left[\frac{f_p}{\left(\frac{G}{10}\right)^{1/6}} - X\right] \tag{4-51}$$

where h_p and f_p are function defined on p. 51 of TRAC P1A manual (1) and

$$n = \begin{cases} 0.4 \text{ for } D \geq 0.01 \text{ m} \\ \\ 0.6 \text{ for } D < 0.01 \text{ m} \end{cases} \tag{4-52}$$

D = diameter (m)

G = mass flux (kg/m^2s)

For the fuel rods inside the channel component, the CISE-GE critical quality correlation (25) shown below is used for the boiling transition criterion in cocurrent upflow situations.

$$*X_c = \frac{AL_B}{B + L_B} \left(\frac{1.24}{F_L}\right)^{1/2} \tag{4-53}$$

where

$$A = 1.055 - 0.013 \left(\frac{p - 4.137 \times 10^6}{2.758 \times 10^6}\right)^2$$

$$- 0.909 \left(\frac{G}{10^3}\right) + 0.493 \left(\frac{G}{10^3}\right)^2 - 0.114 \left(\frac{G}{10^3}\right)^3 \tag{4-54}$$

in which p = pressure (N/m^2)

*New model for TRAC.

$$B = 0.457 + \left(\frac{G}{10^3}\right) - 0.489 \left(\frac{G}{10^3}\right)^2 \qquad (4\text{-}55)$$

in which

G = mass flux (kg/m^2-s)

F_L = local peaking factor on heater rod under consideration

L_B = boiling length (m).

During dryout, the wall heat transfer will remain in nucleate boiling model until the local flow quality is higher than the critical quality, X_c, predicted by the CISE-GE correlation. It is then immediately followed by film boiling without going through the transition boiling regime. Although the approach used here is conservative, it will still simulate the real physical situation very closely. Experimental observations show that as the dryout front propagates, the heat transfer coefficient away from the front drops to film boiling values at fairly low wall superheat.

During rewet, the wall heat transfer will be in the film boiling mode until the wall temperature is lower than the minimum film boiling temperature and the local flow quality is lower than the critical quality. It is then followed by transition boiling. The heat transfer coefficient used in the transition boiling regime is the same as that used by all other components.

4.1.3 Determination of T_{CHF} and T_{min}

The CHEN correlation for the nucleate boiling heat transfer coefficient is used to calculate the surface temperature corresponding to the critical heat flux (CHF) such that

$$T_{CHF} = T_s + \frac{q''_{CHF}}{h_{CHEN}} \qquad (4\text{-}56)$$

is satisfied. Since h_{CHEN} is a function of the wall temperature, an iteration scheme is used to evaluate T_{CHF}.

Two correlations for the minimum stable film temperature, namely the Iloeje correlation and the homogeneous nucleation correlation, are incorporated in the BWR version of TRAC.

The Iloeje correlation (26) is based on Berenson's minimum pool film boiling temperature correlation and extended to provide the effect of mass flux and equilibrium quality. The correlation is given by

$$\Delta T_{min} = T_{min} - T_{sat}$$

$$= 0.29\ \Delta T_{BER}\left(1 - 0.295\ X_E^{2.45}\right)\left(1 + (7.37 \times 10^{-2} G)^{0.49}\right) \qquad (4\text{-}57)$$

where

$$\Delta T_{BER} = 0.127\ \frac{\rho_g}{k_g}\ h_{fg}\left[\frac{g(\rho_\ell - \rho_g)}{\rho_\ell + \rho_g}\right]^{2/3}\left[\frac{\sigma}{g(\rho_\ell - \rho_g)}\right]^{1/2}\left[\frac{\mu_g}{g(\rho_\ell - \rho_g)}\right]^{1/3} \qquad (4\text{-}58)$$

X_E = Equilibrium quality

G = mass flux (kg/m^2s)

In the homogeneous nucleation correlation (27), the minimum stable film temperature, T_{min}, is given by

$$T_{min} = T_{HN} + (T_{HN} - T_\ell)\left(\frac{\rho_\ell k_\ell C_{p,\ell}}{\rho_w k_w C_{p,w}}\right)^{1/2} \qquad (4\text{-}59)$$

For simplicity, the homogeneous nucleation temperature, T_{HN}, is taken to be equal to the critical temperature of water, T_{crit}. The subscript w stands for wall material properties that depend on the surface conditions, i.e., oxidation, crud formation, aging, etc. However, these effects are not included at present.

The effect of the CISE-GE model and the minimum stable film boiling temperature can be seen in the comparison of the Blowdown Heat Transfer (BDHT) experiment (4904R45) (28) with TRAC shown in Figures 4-4 through 4-7. The main parameters for the experiment are given in Table 4-1.

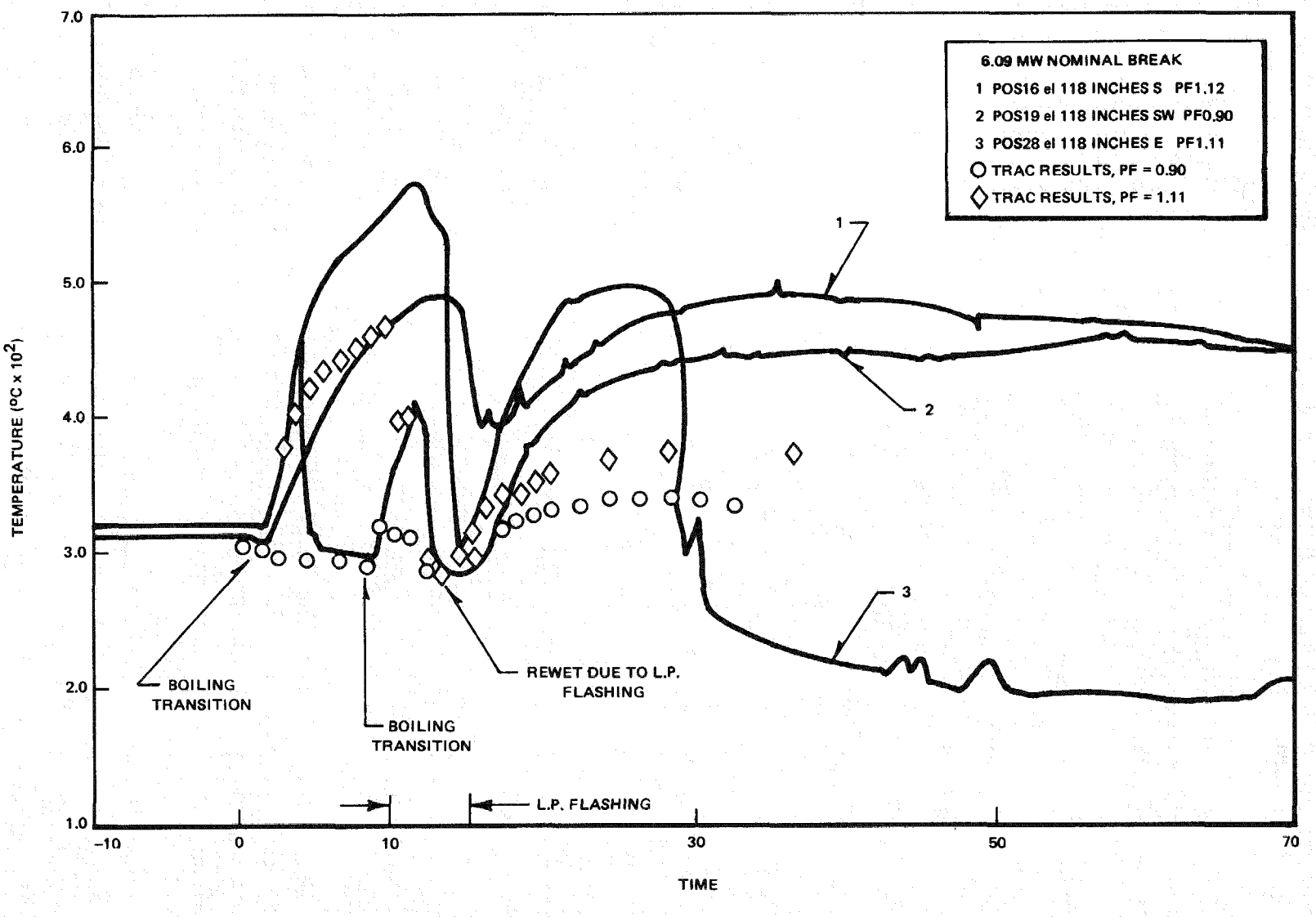

Figure 4-4. Comparison of BDHT Results with TRAC, Elevation 118 inches

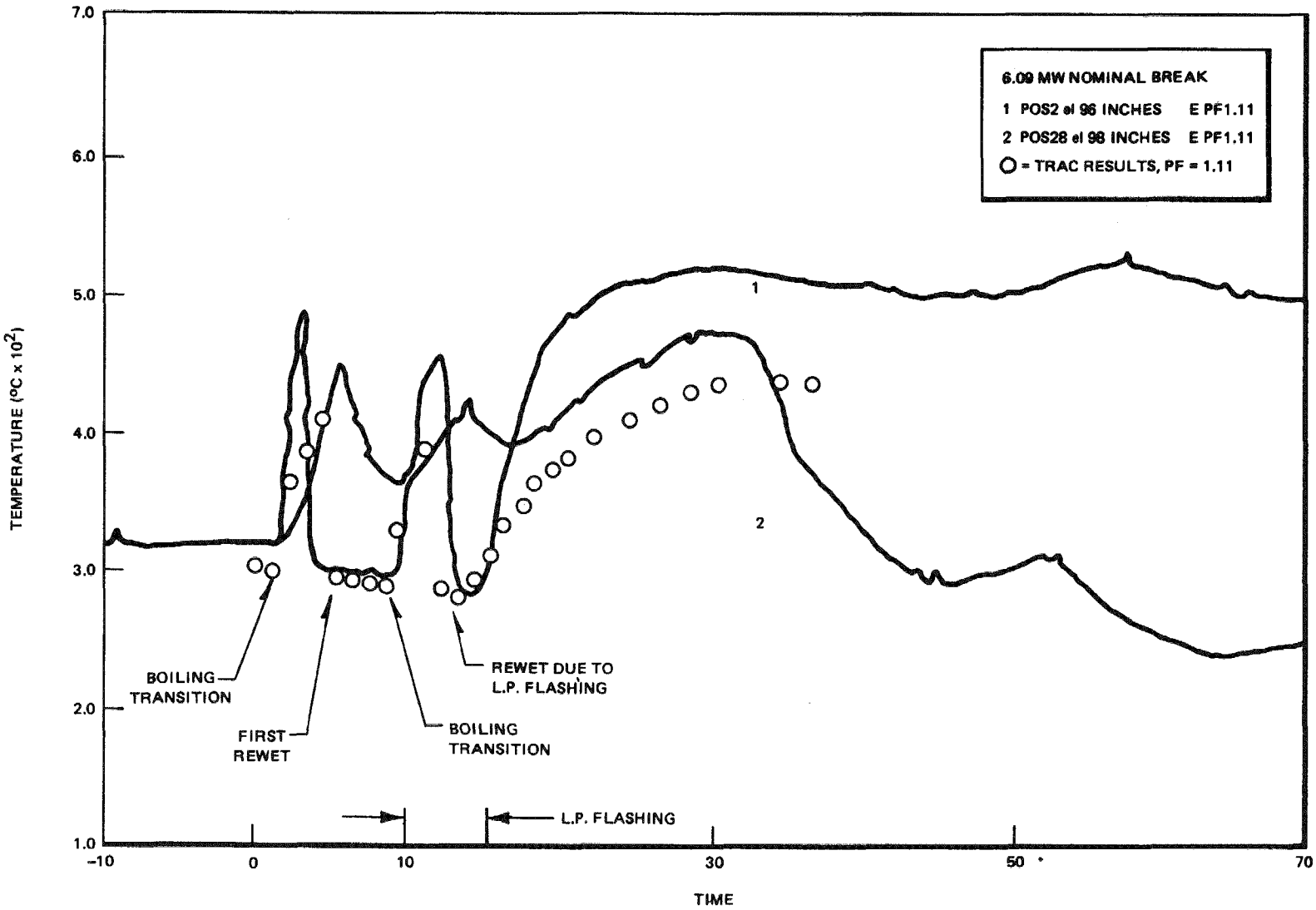

Figure 4-5. Comparison of BDHT Results with TRAC, Elevation 96 and 98 inches

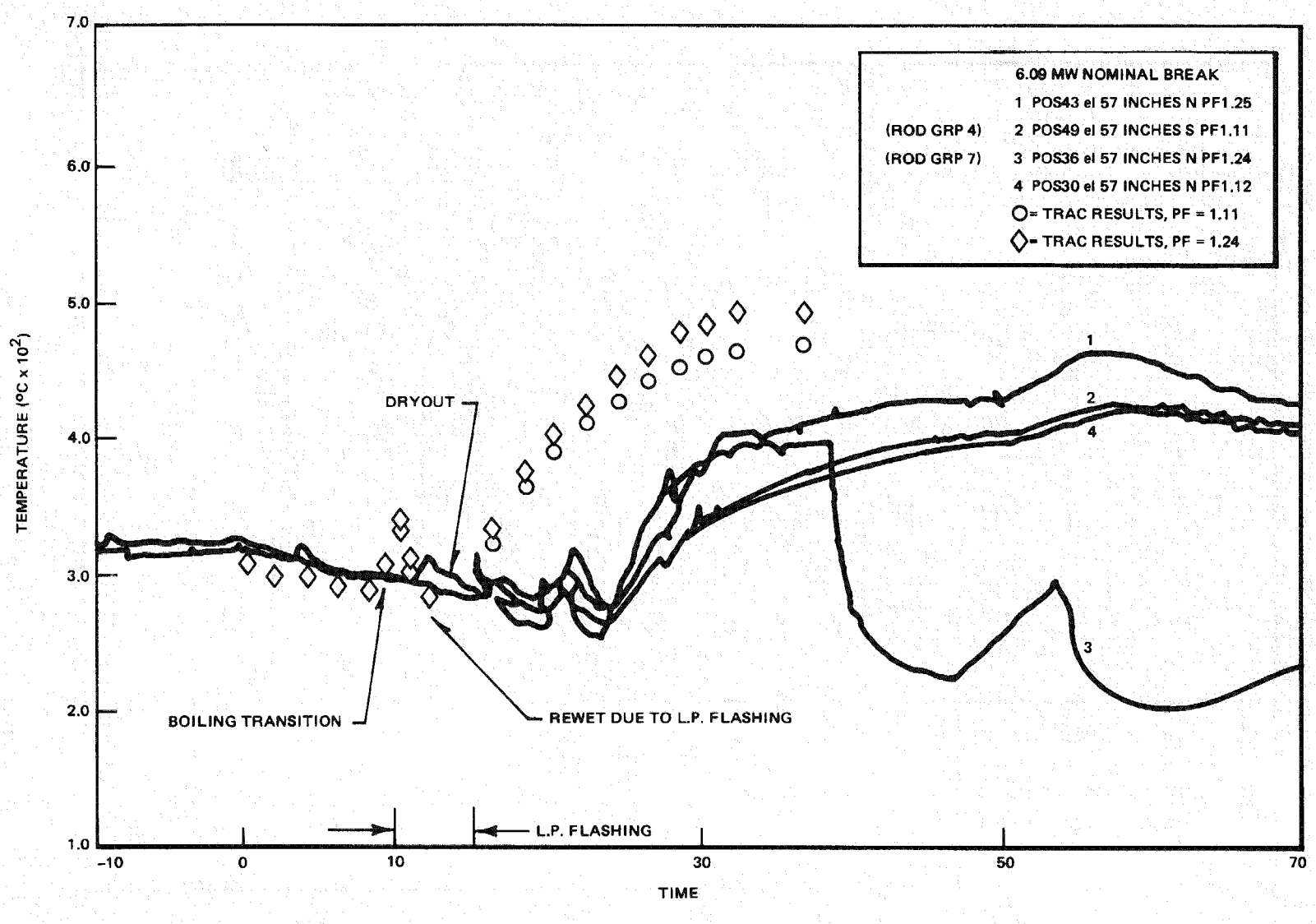

Figure 4-6. Comparison of BDHT Results with TRAC, Elevation 57 inches

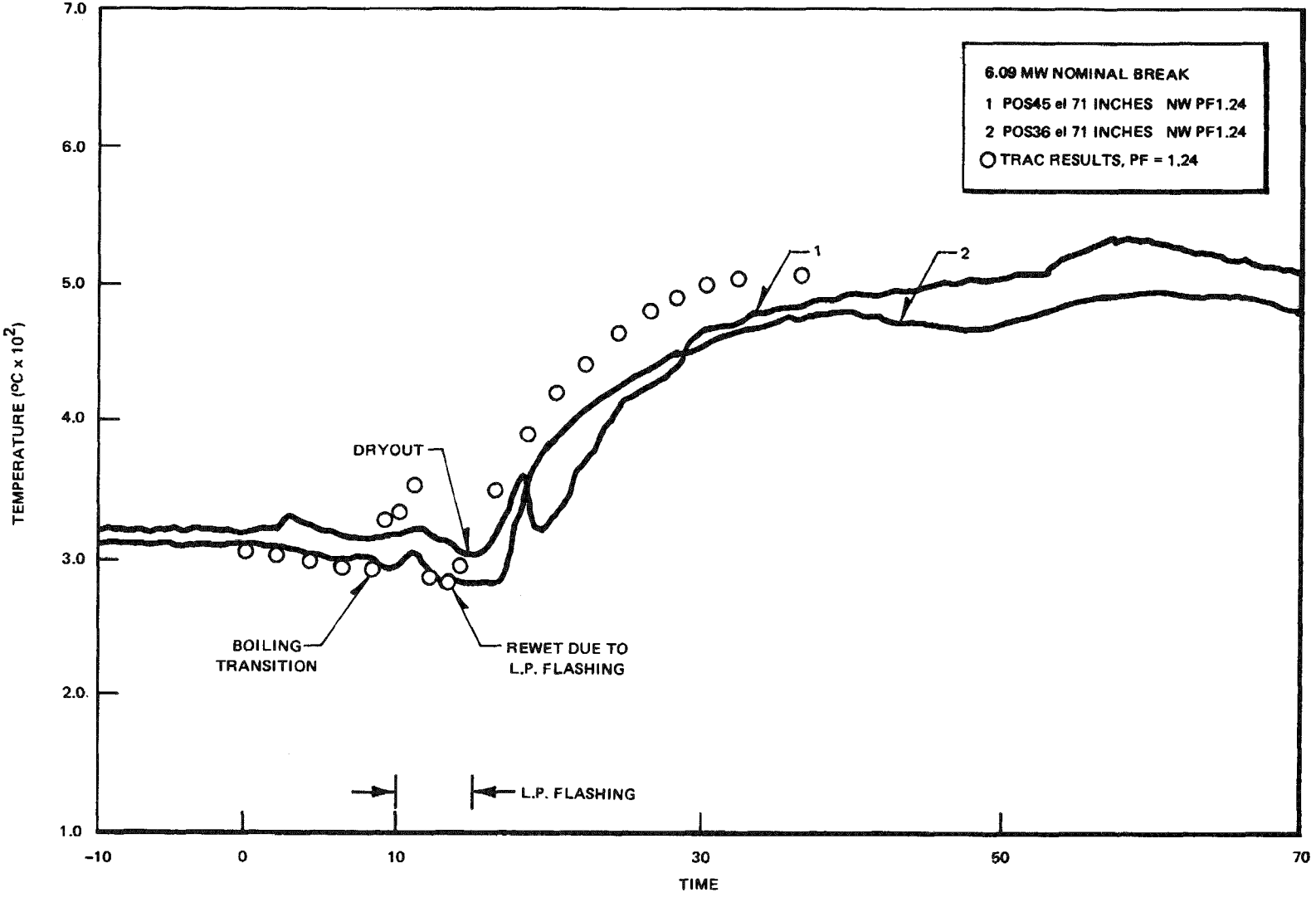

Figure 4-7. Comparison of BDHT Results with TRAC, Elevation 71 inches

Table 4-1

KEY PARAMETERS FOR BDHT (4904R45)

Initial Power	6.042×10^6 W
Number of Rods	49
Rod Diameter	7.144×10^{-3} m
Low Plenum Flashing Time	∿12 sec
Spray Flowrate	∿1 kg/sec
Spray Water Temperature	561°K
Channel Length	3.66 m
Channel Flow Area	0.01 m^2
Break Pressure	7.21×10^6 N/m^2

Power Table

Seconds	Watts
0.0	6.047×10^6
4.8	3.680×10^6
8.3	2.740×10^6
14.0	1.700×10^6
20.0	1.000×10^6
33.0	0.338×10^6
45.0	0.200×10^6

4.2 INTERFACIAL HEAT TRANSFER

The interfacial heat transfer coefficients used in TRAC are obtained as functions of the flow regime. A simple flow regime map (Figure 4-8) based on the cell-centered void fraction is used by all components. It has a transition region between the bubbly and slug flow regime in the mass flux direction and another between the slug or bubbly flow and the annular mist regime in the void fraction direction. In both of these transition regions, a linear interpolation function based on either the mass flux or the void fraction is used (see Section 4.2.4). For a given void fraction, α, the interfacial heat transfer coefficient is found in the manner illustrated in Figure 4-9.

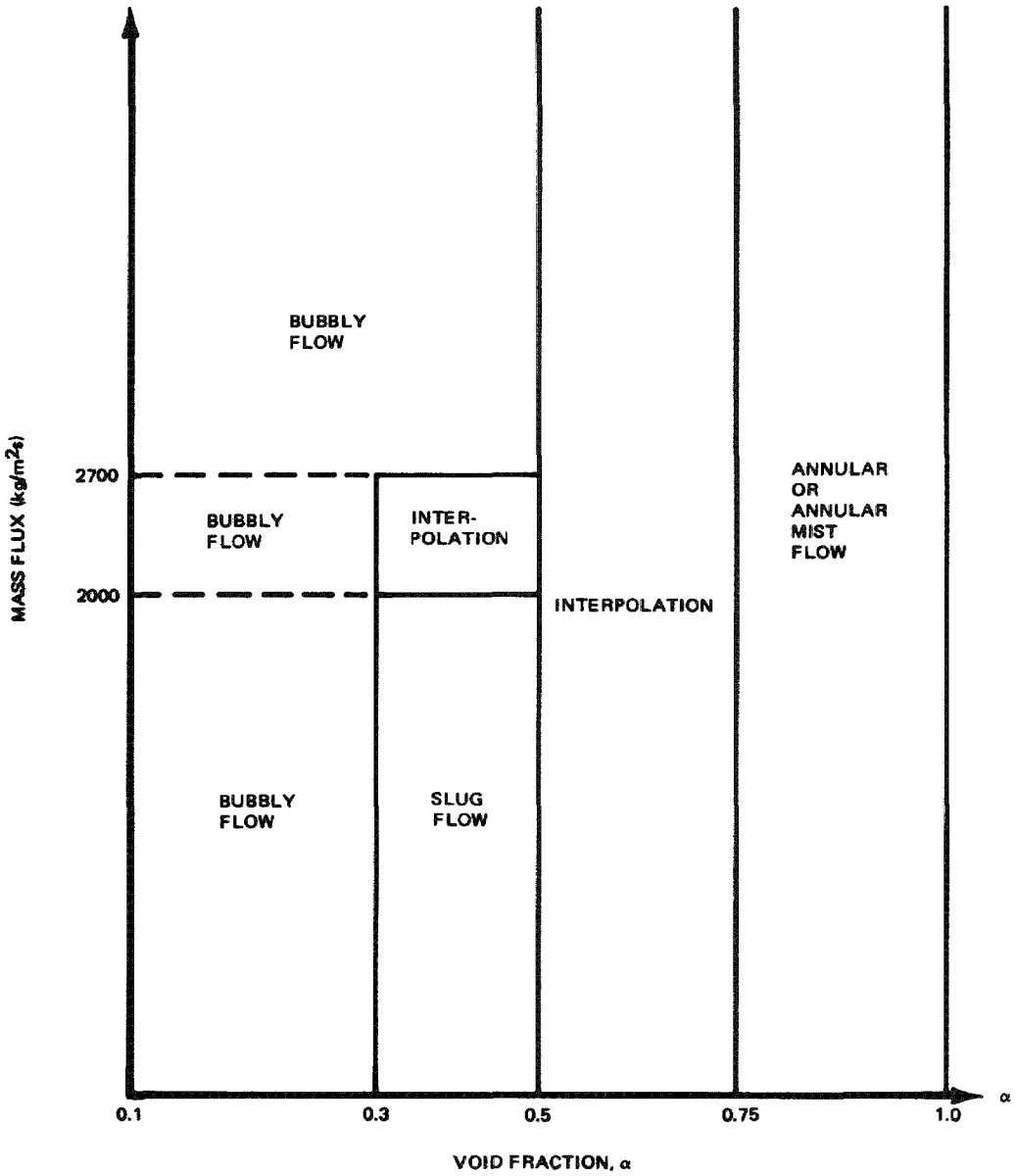

Figure 4-8. Flow Regime Map Based on the Cell-Centered Void Fraction

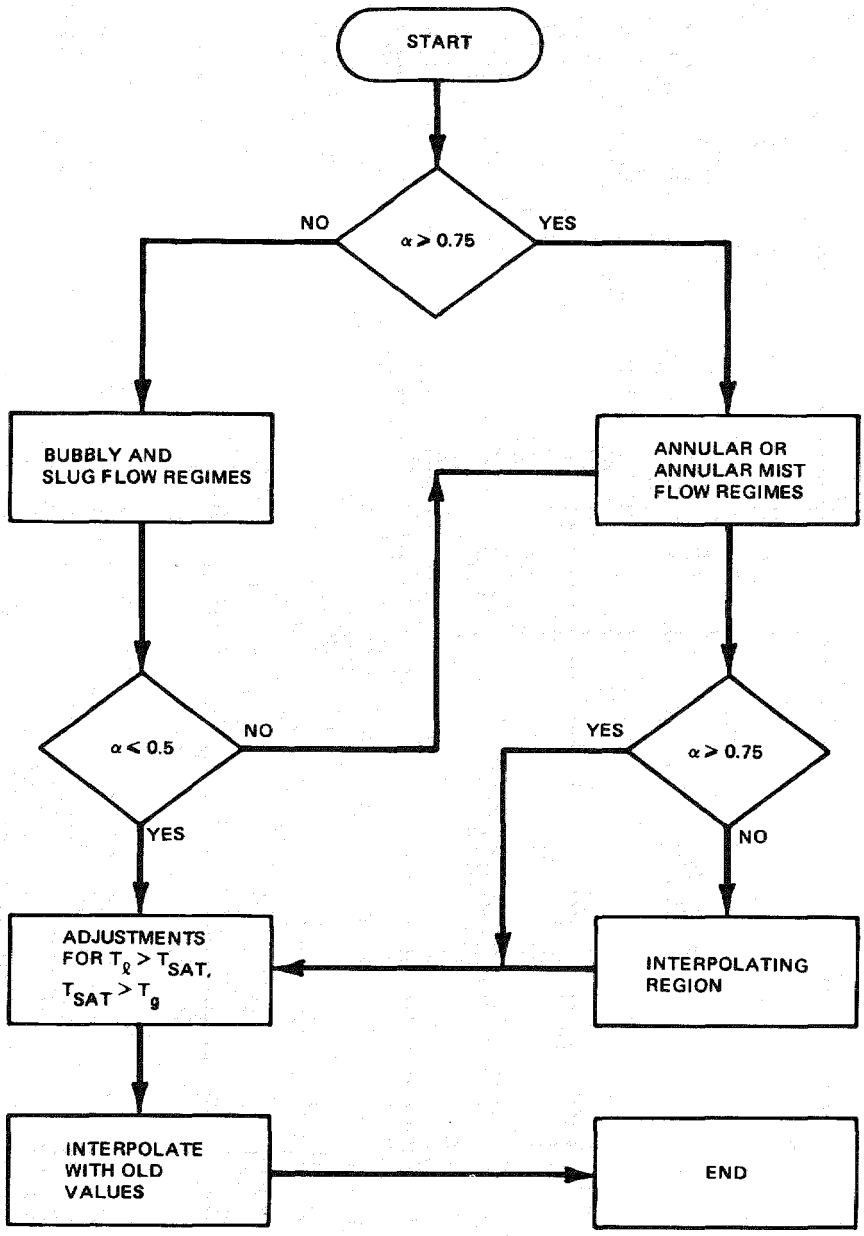

Figure 4-9. Flow Chart for Interfacial Heat Transfer Coefficient

4.2.1 Liquid/Vapor Mass Exchange Model

Mass transfer between phases takes place at the interface and is related to the heat transfer rates as follows:

$$\Gamma_g = \frac{-q_{ig} - q_{i\ell}}{h_{fg}} \tag{4-60}$$

where Γ_g is the vapor generation rate and h_{fg} is the latent heat of evaporation. $q_{i\ell}$ and q_{ig} are the heat transfer rates from interface to vapor and liquid, respectively, and are related to the interfacial heat transfer coefficients according to:

$$q_{i\ell} = h_{i\ell} A_i (T_s - T_\ell) \tag{4-61}$$

$$q_{ig} = h_{ig} A_i (T_s - T_g) \tag{4-62}$$

where A_i is the interfacial area and $h_{i\ell}$ and h_{ig} are the interfacial heat transfer coefficients on the liquid and vapor side respectively.

4.2.2 Annular and Annular Mist Flow Regime ($\alpha > 0.75$)

The fraction of liquid which is entrained in droplet form, E, is computed according to the Steen-Wallis correlation (5).

The interfacial area from the film at the wall is calculated according to

$$A_f = 5(1-E)\,\pi D(\Delta Z) \tag{4-63}$$

where D and ΔZ are the hydraulic diameter and the height of the cell respectively.

The expression used to calculate the total interfacial area of the droplets is

$$A_d = E(1-\alpha)\,V\,\frac{4\pi\left(\frac{D_d}{2}\right)^2}{\frac{4}{3}\pi\left(\frac{D_d}{2}\right)^3} \tag{4-64}$$

$$= 6E(1-\alpha)\,\frac{V}{D_d} \tag{4-65}$$

where the droplet diameter, D_d, is determined from a critical Weber number, We_d.

The total heat transfer coefficient from interface to liquid for the film is calculated from

$$H_{i\ell,f} = A_f \, h_{i\ell,f} \tag{4-66}$$

$$h_{i\ell,f} = 0.0073 \rho_\ell V_r \, c_{p,\ell} \tag{4-67}$$

and from interface to vapor from

$$H_{ig,f} = A_f \, h_{ig,f} \tag{4-68}$$

$$h_{ig,f} = 0.0073 \rho_g V_r \, c_{p,g} \tag{4-69}$$

where V_r is the absolute value of the relative velocity.

The total heat transfer coefficient from interface to liquid from the droplets is calculated from

$$H_{i\ell,d} = A_d \, h_{i\ell,d} \tag{4-70}$$

$$h_{i\ell,d} = 1500 \, \frac{k_\ell}{D_d} \tag{4-71}$$

and from interface to vapor from

$$H_{ig,d} = A_d \, h_{ig,d} \tag{4-72}$$

$$h_{ig,d} = Nu_d \, \frac{k_g}{D_d} \tag{4-73}$$

$$Nu_d = 2 + 0.74 \left(\frac{P_g \, V_R \, D_d}{\mu_g} \right)^{1/2} Pr_g^{1/3} \tag{4-74}$$

4.2.3 Bubbly Flow and Slug Flow Regimes ($\alpha \leq 0.5$)

The bubble and slug volume fractions are determined from the interpolating functions shown in Figure 4-10. The flow will be a pure bubbly flow when $\alpha < 0.3$ and will become a mixture of bubbly and slug flow when α is between 0.3 and 0.5. The mass flux will also have an effect on the bubble and slug volume fraction. Under any circumstances at least 20% of the vapor will appear as trailing bubbles.

The interfacial area for the slug and the bubble is calculated from:

$$A_S = 5\,\alpha_S\,\frac{V}{D} \tag{4-75}$$

$$A_B = 6\,\alpha_B\,\frac{V}{D_B} \tag{4-76}$$

where D_B is the bubble diameter determined from a critical Weber number.

The total heat transfer coefficients from interface to liquid for the bubble is calculated from

$$H_{i\ell,B} = A_B\,h_{i\ell,B} \tag{4-77}$$

$$h_{i\ell,B} = \max\{h_1,\ h_2\} \tag{4-78}$$

$$h_1 = \frac{k_\ell}{D_B}\left[2 + 0.74\left(\frac{P_\ell v_r D_B}{\mu_\ell}\right)^{1/2}\right] \tag{4-79}$$

$$h_2 = \frac{k_\ell}{D_B}\left\{\frac{3.82(T_\ell - T_s)\,\rho_\ell C_{p.\ell}}{\rho_g(h_{sg} - h_{s\ell})}\right\} \tag{4-80}$$

and for the slug from

$$H_{i\ell,s} = A_s\,h_{i\ell,s} \tag{4-81}$$

$$h_{i\ell,s} = 0.0073\,\rho_\ell v_r\,C_{p,\ell} \tag{4-82}$$

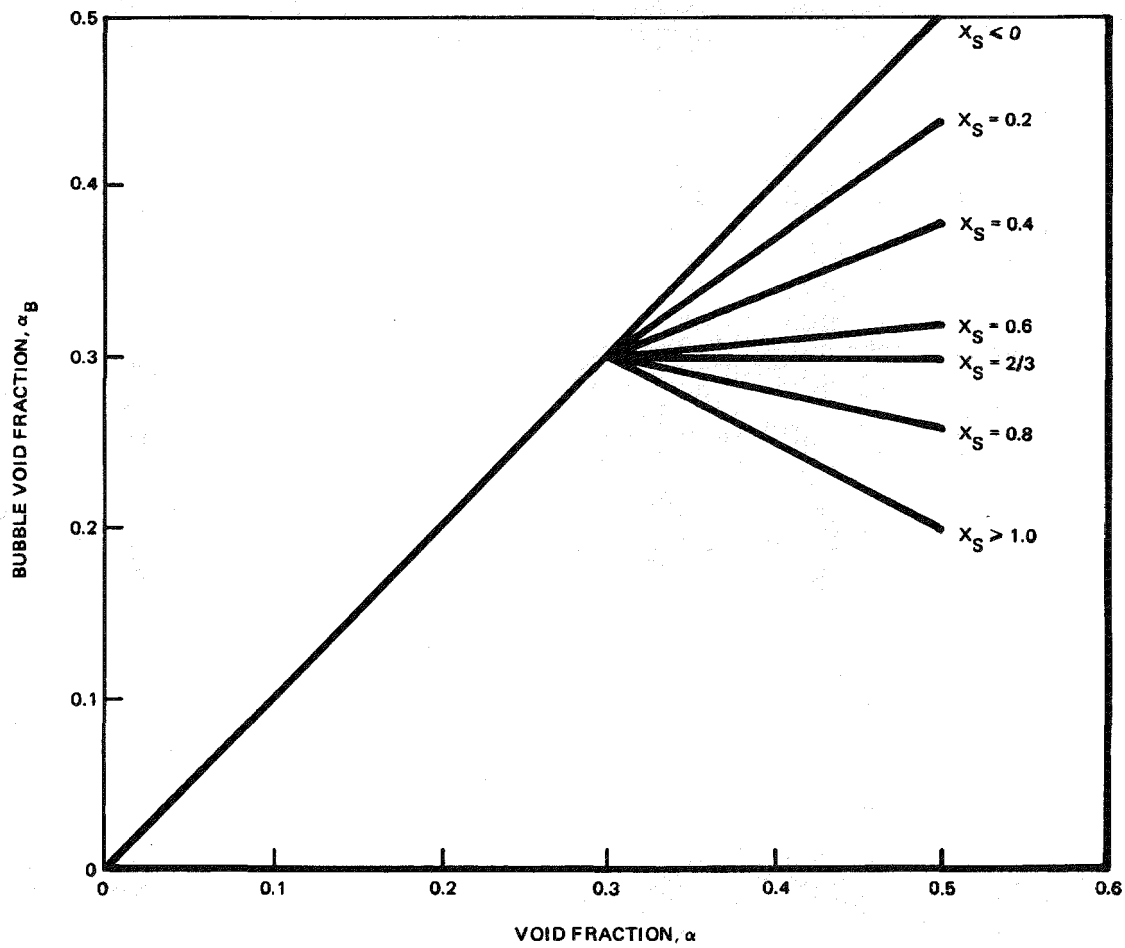

$$\alpha_B = \alpha(1 - X_S) + (0.45 - 5\alpha) X_S$$

$$3 < 2 < 0.5$$

$$0 < X_S < 1$$

$$x_s = \frac{2700 - G}{2700 - 2000} \quad \text{FOR } 3 < \alpha < 0.5$$

Figure 4-10. Bubble and Slug Volume Fractions

The total heat transfer coefficient from interface to vapor is calculated from

$$H_{ig} = \text{Max}\left\{V \times 10^7, H_{ig}'\right\} \tag{4-83}$$

$$H_{ig}' = (A_D + A_S)\, 10^4 \tag{4-84}$$

4.2.4 Interpolation Region ($0.5 < \alpha < 0.75$)

The interfacial heat transfer coefficients in this region is obtained by interpolating the interfacial heat transfer coefficients at $\alpha = 0.5$ and 0.75, as follows:

$$H_{i\ell}(\alpha) = 4\alpha\left[H_{i\ell}(0.75) - H_{i\ell}(0.5)\right] + 3H_{i\ell}(0.5) - 2H_{i\ell}(0.75) \tag{4-85}$$

$$H_{ig}(\alpha) = 4\alpha\left[H_{ig}(0.75) - H_{ig}(0.5)\right] + 3H_{ig}(0.5) - 2H_{ig}(0.75) \tag{4-86}$$

The relative velocity of the bubble is also interpolated as follows:

$$v_{rB} = 4\,(v'_{rB} - v_r)\alpha + 3v_r - 2v'_{rb} \tag{4-87}$$

$$v'_{rB} = 3.06\left[\frac{g\sigma\,(\rho_\ell - \rho_g)}{\rho_\ell^2}\right]^{1/4} \tag{4-88}$$

4.2.5 Subcooled Boiling Effect

During subcooled boiling, vaporization may occur at the heated surface despite the fact that the mean temperature of the cooling liquid has not yet reached the saturation point. This phenomenon is caused by a nonuniform temperature distribution in the liquid.

In the BWR version of TRAC, each computing cell is assumed to have a uniform temperature distribution and the volumetric vaporization rate is modeled as

$$\Gamma_g = -\frac{q_{i\ell} + q_{ig}}{h_{fg}} \tag{4-89}$$

where

$$q_{i\ell} = A_i\, h_{i\ell}\, (T_s - T_\ell) \tag{4-90}$$

$$q_{ig} = A_i\, h_{ig}\, (T_s - T_g) \tag{4-91}$$

This means no vapor will be generated until the liquid reaches its saturation point and the void fraction will not be correctly predicted during subcooled boiling.

The Rouhani-Bowring model (29) for subcooled boiling energy distribution along with the Saha-Zuber model (30) for subcooled boiling initiation were used to improve the subcooled boiling results from TRAC. The models can be summarized by the following equations:

- Rouhani-Bowring Model

$$q_w = \text{heat flux at the wall}$$

$$= q_\ell + q_{evap} \tag{4-92}$$

where

q_ℓ = Heat flux from the wall, which goes to heat up the liquid

$$= \begin{cases} q_w \quad \text{if} \quad h_\ell \le h_{\ell d} & (4\text{-}93) \\ q_w \dfrac{h_{\ell s} - h_\ell}{h_{\ell s} - h_{\ell d}} + q_w \left(1 - \dfrac{h_{\ell s} - h_\ell}{h_{\ell s} - h_{\ell d}}\right) \dfrac{\varepsilon}{1 + \varepsilon} & (4\text{-}94) \end{cases}$$

q_{evap} = Heat flux which goes to vaporize the liquid

$$= (q_w - q_\ell) \tag{4-95}$$

ε = Pumping factor

$$= \frac{\rho_\ell\, (h_{\ell s} - h_\ell)}{\rho_g h_{fg}} \tag{4-96}$$

- Saha-Zuber Model

$h_{\ell d}$ = Subcooled bubble departure enthalpy

$$= \begin{cases} h_{\ell s} - 154 \dfrac{q_w}{\rho_\ell v_\ell} & \text{if } Pe < 70000 \\ h_{\ell s} - 0.0022 \dfrac{q_w D_h C_{p,\ell}}{k_\ell} & \text{if } Pe \leq 70000 \end{cases} \quad (4\text{-}97)$$

where

$$P_e = \frac{G_\ell D_H C_{p,\ell}}{k_\ell} \quad (4\text{-}98)$$

The expression for $q_{i\ell}$ is the modified to

$$q_{i\ell} = A_i h_{i\ell} (T_s - T_\ell) - A_w q_{evap} \quad (4\text{-}99)$$

Hence vapor will be generated even if the liquid temperature is below saturation temperature.

The effect of the subcooled boiling model is illustrated in Figure 4-11. The test conditions are summarized in Table 4-2.

Table 4-2

KEY PARAMETERS FOR SUBCOOLED BOILING TEST

Mass Flux	1050 kg/m^2s
Wall Heat Flux	0.9 MW/m^2
Inlet Subcooling	30°K
Ambient Pressure	$5x10^6$ N/m^2
Pipe Diameter	3.7×10^{-2} m

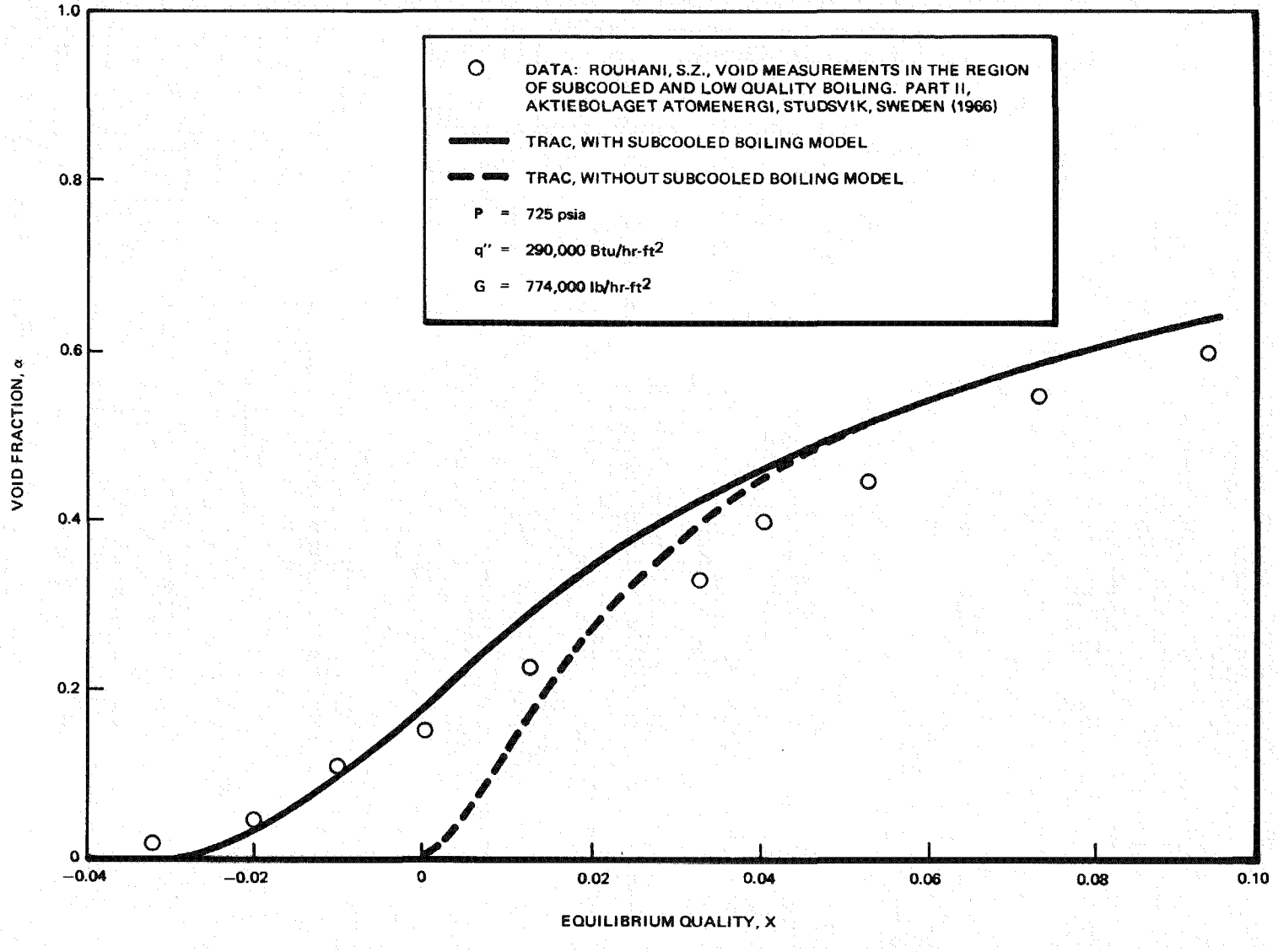

Figure 4-11. Comparison of TRAC Results and Void Fraction Data

4.3 THERMAL RADIATION

During a loss-of-coolant accident for a boiling water reactor, radiation heat transfer may account for a significant amount of the total heat transfer in the fuel bundle. An analytical model for calculating radiation heat transfer in a BWR fuel bundle was established and implemented into the BWR version of TRAC. The model considers surface-to-surface radiation and the interaction between radiation and the two-phase mixture in the bundle. The surface-to-surface radiation model contains a first-order anisotropic transport correction, and the interaction with the two-phase mixture consists of absorption and emission.

4.3.1 Radiation Heat Transfer Model

The radiation heat transfer mode (31)* is based on the following assumptions:

- All surfaces are gray
- All surfaces have uniform temperatures
- All surfaces emit radiation diffusely
- The two-phase flow between surfaces has uniform temperature, and it absorbs and emits radiation
- The semi-gray radiation model holds for the two-phase mixture; i.e., absorption is based on the wall temperature, while emission is based on the temperature of the two-phase mixture
- The first-order anisotropic transport correction holds for surface reflection

For large and/or curved surfaces, there is generally a tendency for radiation to be reflected backwards towards the origin of the incident radiation. Hence, the assumption that a fraction, μ, of the incident radiation is reflected backwards toward the origin, whereas the rest, $1-\mu$, is reflected uniformly in all directions, is a significant improvement over the assumption of isotropic reflection.

The radiosity of surface i, B_i can be expressed as the sum of the emitted and reflected radiation (see Figure 4-12).

$$B_i = \varepsilon_i S_i + (1-\varepsilon_i) H_i \qquad (4\text{-}100)$$

*New model for TRAC

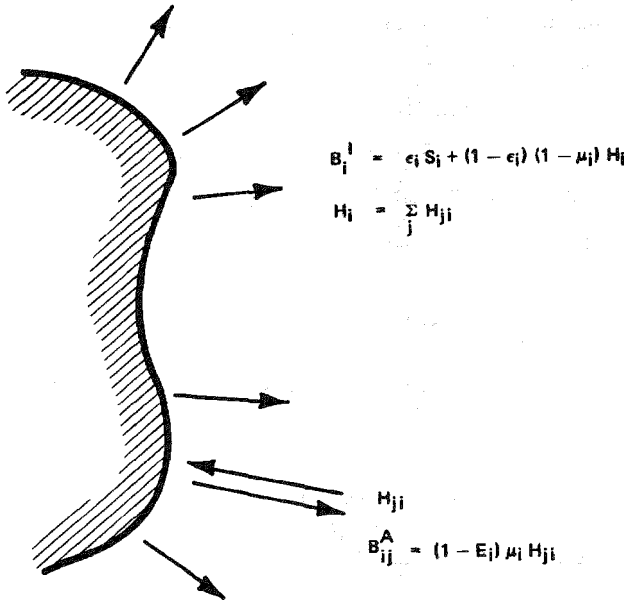

Figure 4-12. Radiation Heat Fluxes at a Surface

where

ε_i = Emissivity of surface i

$$S_i = \sigma T_i^4 \tag{4-101}$$

$$H_i = \sum_j H_{ji} \tag{4-102}$$

and H_{ji} is the incident radiation of surface i coming from surface j.

The isotropic part of the radiosity of surface i, B_i^I, is given by

$$B_i^I = \varepsilon_i S_i + (1 - \varepsilon_i)(1 - \mu_i) H_i \tag{4-103}$$

and the anisotropic part, B_{ij}^A, which is reflected back to surface j, is

$$B_{ij}^A = \mu_i (1-\varepsilon_i) H_{ji} \tag{4-104}$$

The incident radiation from the direction of surface j is the sum of the radiation leaving surface j in the direction of surface i reduced by the transmissivity of the medium plus what is emitted by the medium,

$$H_{ji} = \frac{1}{A_i}\left(A_j B_j^I F_{ji} + A_j B_{ji}^A\right) \tau_{ji} \tag{4-105}$$

After some lenghly algebraic manipulations, the following expression is obtained:

$$B_{ij}^A = \left(a_{ij} B^I + b_{ij} B_j^I + c_{ij}\right) F_{ij} \tag{4-106}$$

where

$$a_{ij} = \frac{X_i X_i t_{ij} t_{ji}}{1 - X_i X_j t_{ij} t_{ji}} \tag{4-107}$$

$$b_{ij} = \frac{X_i t_{ji}}{1 - X_i X_j t_{ij} t_{ji}} \tag{4-108}$$

$$c_{ij} = \frac{X_i(\varepsilon_{mij} S_{mij} + X_j t_{ji} \varepsilon_{mji} S_{mji})}{1 - X_i X_j t_{ij} t_{ji}} \tag{4-109}$$

$$X_i = \mu_i (1-\varepsilon_i) \tag{4-110}$$

$$t_{ij} = e^{-(a_{\ell ij} + a_{gij}) R_{ij}} \tag{4-111}$$

$$\varepsilon_{mij} = \varepsilon_{\ell ij} + \varepsilon_{gij} \tag{4-112}$$

$$S_{mij} = \frac{\varepsilon_{\ell ig} S_\ell + \varepsilon_{gij} S_g}{\varepsilon_{\ell ij} + \varepsilon_{gij}} \tag{4-113}$$

$$S_\ell = \sigma T_\ell^4 \tag{4-114}$$

$$S_g = \sigma T_g^4 \tag{4-115}$$

$$\varepsilon_{\ell ij} = \frac{a_\ell}{a_\ell + a_g}\left[1 - e^{-(a_\ell + a_g)R_{ig}}\right] \quad (4\text{-}116)$$

$$\varepsilon_{gij} = \frac{a_g}{a_\ell + a_g}\left[1 - e^{-(a_\ell + a_g)R_{ig}}\right] \quad (4\text{-}117)$$

$$a_{\ell ij} = \frac{a_{\ell,i}\, S_i + a_{\ell,j}\, S_j}{S_i + S_j} \quad (4\text{-}118)$$

$$a_{gij} = \frac{a_{g,i}\, S_i + a_{g,i}\, S_j}{S_i + S_i} \quad (4\text{-}119)$$

$a_{g,i}$ = Vapor absorption coefficient evaluated at temperature of surface i

$$= f_g\,(T_i) \quad (4\text{-}120)$$

$a_{\ell,i}$ = Liquid absorption coefficient evaluated at temperature of surface i

$$= f_\ell\,(T_i) \quad (4\text{-}121)$$

$$a_g = f_g\,(T_g) \quad (4\text{-}122)$$

$$a_\ell = f_\ell\,(T_\ell) \quad (4\text{-}123)$$

T_i = Temperature of surface i (°K)

T_g = Temperature of steam (°K)

T_ℓ = Temperature of liquid (°K)

$$f_\ell = 1.11\,(1-\alpha)/d_d \quad (4\text{-}124)$$

$$f_g = P\,\{5.2 \times 10^4 - 9 \times 10^{-19}T + 5.6 \times 10^{-10}T^2 - 1.2 \times 10^{-13}T^3\} \quad (4\text{-}125)$$

α = Void fraction

P = Pressure (N/m^2)

d_d = Droplet diameter

R_{ij} = Mean beam length between surfaces i and j.

Combining Eqs. 4-102, 4-103, 4-104, and 4-36, the following expression is obtained

$$B_i^I = \epsilon_i S_i + \frac{1 - \mu_i}{\mu_i} \sum_j \left(a_{ij} B_i^I + b_{ij} B_j^I + c_{ij}\right) F_{ij} \qquad (4\text{-}126)$$

This is a system of linear equations, which can be solved for B_i^I.

The surface heat flux of surface, i, is the difference between the radiosity and incident radiation,

$$q_i = B_i - H_i \qquad (4\text{-}127)$$

Combining Eqs. 4-100, 4-103, and 4-127 yields,

$$q_i = \frac{\epsilon_i}{1 - \epsilon_i} \frac{S_i[1-\mu_i(1-\epsilon_i)] - B_i^I}{1 - \mu_i} \qquad (4\text{-}128)$$

The energy absorbed and emitted by steam are given by the following equations:

$$Q_{abs,g} = \sum_i \sum_j A_i \left(F_{ij} B_i^I + B_{ij}^A\right) \left(1-t_{ij}\right) \frac{a_{gij}}{a_{gij} + a_{\ell ij}} \qquad (4\text{-}129)$$

and

$$Q_{emit,g} = \sum_i \sum_j A_i \, \epsilon_{m_{ij}} \frac{\epsilon_{g_{ij}} S_g}{\epsilon_{g_{ij}} \epsilon_{\ell_{ij}}} F_{ij} \qquad (4\text{-}130)$$

Similar expressions can be written for the absorption and emission for the liquid. Energy conservation can be shown by

$$\sum_i Q_i = Q_{abs,\ell} + Q_{abs,g} - Q_{emit,g} - Q_{emit,\ell} \tag{4-131}$$

after simple but tedious algebraic manipulations.

Net heat fluxes from surface i to either steam or liquid can be derived from Eqs. 4-129 and 4-130, as follows:

$$q_{i,g} = \sum_j \left\{ \left(F_{ij}B_i^I + B_{ij}^A\right)\left(1-t_{ij}\right) \frac{a_{g_{ij}}}{a_{g_{ij}} + a_{\ell_{ij}}} - F_{ij}\,\varepsilon_{g_{ij}}\,S_g \right\} \tag{4-132}$$

$$q_{i,\ell} \quad \sum_j \left\{ \left(F_{ij}B_i^I + B_{ij}^A\right)\left(1-t_{ij}\right) \frac{a_{\ell_{ij}}}{a_{g_{ij}} + a_{\ell_{ij}}} - F_{ij}\,\varepsilon_{\ell_{ij}}\,S_\ell \right\} \tag{4-133}$$

A comparison between TRAC and the data for a radiation only experiment is shown in Figure 4-13.

The data is obtained from the initial heatup run of a spray cooling experiment where the rods were allowed to heat up slowly until thermal equilibrium was reached. The conditions of the test are summarized in Table 4-3.

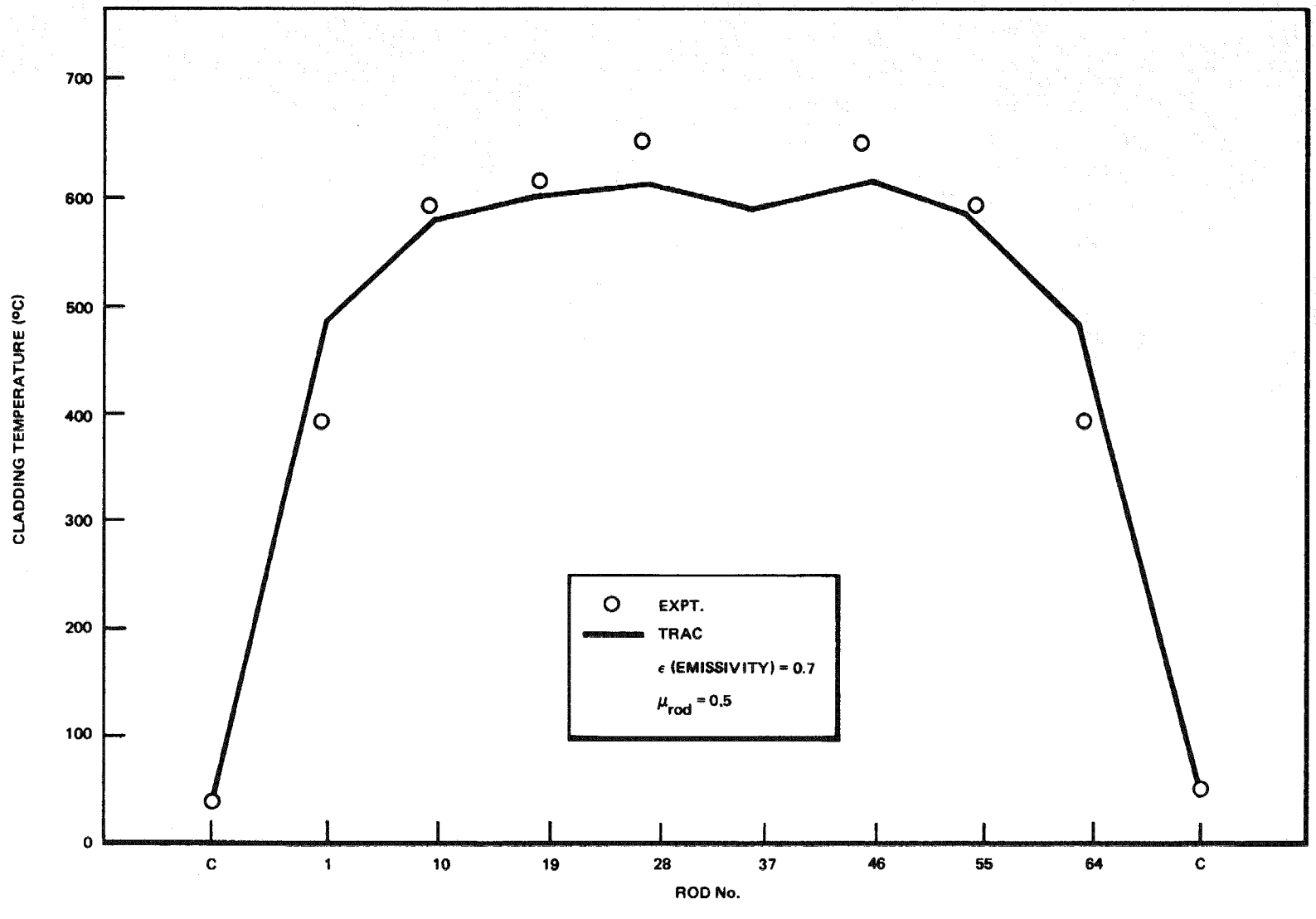

Figure 4-13. Comparison of TRAC Results with Radiation-only Experiment

Table 4-3

KEY PARAMETERS FOR SPRAY COOLING EXPERIMENT

Power	2.5×10^4 W
Ambient Pressure	1.01×10^5 N/m^2
Bundle Length	4.62 m
Flow Area	0.01 m^2
Number of Rods	49
Rod Diameter	6.261×10^{-3} m
Channel Outside Water Temperature	311.5°K

Section 5

CONCLUSION

A methodology for the correlation of the interface shear and wall friction based on void fraction and pressure drop data has been developed, and a set of correlations for the BWR version of TRAC has been developed. Furthermore, the set of heat transfer models in TRAC has been upgraded to cover all the major heat transfer phenomena.

It is realized that there is room for further improvement of the basic models in TRAC, and the future model development will be aimed at the improvement of these models. For the heat transfer, further improvement is required for the transition boiling, film boiling, and interface heat transfer, which includes the condensation heat transfer. Furthermore, the models for the shear should be extended to include inverse annular flow, and correlations for the entrainment and deposition process should be developed. Finally, the need for further improvement of the virtual mass term will be assessed.

However, it is felt that the present set of basic models cover the major phenomena during a BWR LOCA. These models will be thoroughly assessed, and the outcome will guide the future development of TRAC.

Section 6

NOMENCLATURE

A	Flow area (m^2)
A	Surface area (m^2)
a	Absorption coefficient (m^{-1})
a	Constant
B	Radiosity (W/m^2)
B^I	Isotropic radiosity (W/m^2)
B_{ij}^A	Anisotropic radiosity (W/m^2)
c_p	Specific heat capacity ($J/kg°K$)
C	Constant
c	Friction factor
c_o	Distribution parameter
D	Diameter (m)
D_h	Hydraulic diameter (m)
d_i	Interface area/unit volume (m^{-1})
E	Entrainment fraction
e	Specific internal energy (J/kg)
f_i	Induced shear due to phase distribution (kg/m^2s^2)
F	Friction (kg/m^2s^2)
F_{ij}	View factor
F	Reynolds number factor defined on page 54 of TRAC P1A Manual (1)
F_s	Subcooled correction factor defined by Equations 4-16 and 4-48
F_L	Local peaking factor
F	Shear (kg/m^2s^2)
f	Function

G	Mass flux (kg/m^2s)
Gr	Grashof number
g	Acceleration of gravity (m/s^2)
g_c	Gravitational conversion constant
H_{ji}	Irradiation of surface i coming from surface j
H	Total heat transfer coefficient ($W/°K$)
H_i	Total irradiation of surface i (W/m^2)
h	Heat transfer coefficient ($W/m^2°K$)
h	Specific enthalpy (J/kg)
h_{fg}	Heat of evaporization (J/kg)
$h_{\ell d}$	Subcooled bubble departure enthalpy (J/kg)
j	Volumetric flux (m/s)
K	Constant
k	Constant
k	Conductivity ($W/m°K$)
L_B	Boiling length (m)
M	Drag (kg/ms^2)
m	Constant
Nu	Nusselt number
$N_{\mu\ell}$	Viscosity number
$\overline{n}$	Unit vector normal to surface
P	Pressure (N/m^2)
Pe	Peclet number. Defined by Equation 4-98.
Pr	Prandtl number
ΔP	$P_s - P$
q	Heat flux (W/m^3)
Re	Reynolds number
R_{ij}	Beam length (m)
S	Suppression factor defined on page 54 of TRAC P1A Manual (1)

S	Surface area (m^2)
S	Black body radiation (W/m^2)
T	Temperature (°K)
ΔT	$T_w - T_s$
t	Time (s)
V	Cell volume (m^3)
v	Velocity (m/s)
We_c	Critical Weber number
X	Quality
X_{flow}	Flow quality
X_E	Equilibrium quality
X_c	Critical quality
Z	Length (m)

SUBSCRIPTS

B	Bubble
B	Bromley
BER	Berenson
c	Continuous
C	Condensation
CHF	Critical heat flux
CHEN	Chen's correlation
DR	Dougall Rohsenow
D	Drag
di	Dispersed
d	Droplet
evap	Evaporization
f	Film
FORC	Forced convection
FREE	Free convection
g	Vapor
h	Hydraulic
HN	Homogeneous nucleation
i	i^{th} surface
i	Interface
j	Reference to average volumetric flux
ℓ	Liquid
lam	Laminar
m	Two-phase mixture
min	Minimum stable film boiling
NUCL	Nucleate boiling
NC	Natural convection

R	Radiation
r	Relative
s	Saturation
s	Slug
turb	Turbulent
W	Wall
z	Axial direction

GREEK

α	Void fraction
Γ	Vapor generation rate (kg/m^3s)
$\overline{\overline{\tau}}$	Shear tensor (N/m^2)
τ	Transmissivity
η	Constant
μ	Viscosity (kg/ms)
μ	Anisotropic reflectivity
σ	Surface tension (N/m)
ρ	Density (kg/m^3)
β	Thermal expansivity
γ	Defined by Equation 4-22
σ	Stefan-Boltzmann constant ($W/m^2{}^\circ K^4$)
ε	Emissivity
λ	Defined by Equation 4-29
Γ_g, Γ_v	Vapor generation rate (kg/m^3s)

Section 7

REFERENCES

1. R. J. Pryor, et al., TRAC-P1A, An Advanced Best Estimate Computer Program for PWR LOCA Analysis, Los Alamos Scientific Laboratory, May 1979, (NUREG/CR -0665, LA-777-7S).

2. M. M. Aburomia, BWR Refill - Reflood Program TRAC-BWR Component Development, GEAP-24941, May 1981.

3. M. Ishii, One Dimensional Drift-Flux Model and Constitutive Equations for Relative Motion Between Phases in Various Two-Phase Flow Regimes, October 1977, (ANL-77-47).

4. N. Zuber, et al., Steady State and Transient Void Fraction in Two-Phase Flow Systems, General Electric Company, 1967, 1, (GEAP-5417).

5. G. B. Wallis, One Dimensional Two-Phase Flow, McGraw-Hill Book Co., Inc., New York, 1969.

6. N. Zuber and J. A. Findlay, "Average Volumetric Concentration in Two Phase Flow Systems," Journal of Heat Transfer, 1965, 87, p. 453.

7. J. Nikuradse, "Gesetzmäßigkeit der Turbulenten Strömung-in glatten Rohren," Forch. Arb. Ing. Wes., 1932, p.356.

8. G. Agostini, A. Era and A. Premoli, Density Measurement of Steam-Water Mixtures Flowing in a Tubular Channel Under Adiabatic and Heated Conditions, December 1969, (CISE-R-291).

9. Y. Taitel, D. Borvea and A. E. Dukler, "Modeling Flow Pattern Transitions for Steady Upward Gas-Liquid Flow in Vertical Tubes," AICLE Journal, 1980, 26, No. 3, pp. 345-354.

10. M. Ishii and M. A. Grolmes, "Inception Criteria for Droplet Entrainment in Two-Phase Concurrent Film Flow," AIChE 3. 1975, 21, p. 308.

11. M. Ishii and K. Mashima, Correlation for Liquid Entrainment in Annular Two-Phase Flow of Low Viscous Fluid, March 1981, (ANL/KAS/LWR 81-2).

12. D. D. Jones, Subcooled Counter Current Flow Limiting Characteristics of the Upper Region of a BWR Fuel Bundle, General Electric Company, 1977, (NEDG-NUREG-23549).

13. W. M. Rohsenow and H. Y. Choi, Heat, Mass and Momentum Transfer, Prentice-Hall Inc., Englewood Cliffs, New Jersey, 1961.

14. F. W. Dittus and L. M. K. Boelter, University of California, Publication Engineering, 1930, 2, p. 443.

15. J. P. Holman, Heat Transfer, 3rd Edition, McGraw-Hill, New York, 1972.

16. J. C. Chen, "A Correlation for Boiling Heat Transfer of Saturated Fluids in Convective Flow," ASME Paper, 1963, 63-HT-34.

17. R. S. Dougall and W. M. Rohsenow, Film Boiling on the Inside of Vertical Tube With Upward Flow of Fluids at Low Qualities, MIT Mechanical Engineering, 1963, (9079-26).

18. L. A. Bromley, "Heat Transfer in Stable Film Boiling," Chemical Engineering Process, May 1950, 46, pp. 221-227.

19. W. H. McAdams, Heat Transmission, McGraw-Hill Company, New York, 1954, 3rd Edition.

20. E. F. Carpenter and A. P. Colburn, "The Effect of Vapor Velocity on Laminar and Turbulent Film Condensation," Transactions ASME, 1956, 78, pp. 1637-1643.

21. J. C. Chato, "Laminar Condensation Inside Horizontal and Inclined Tubes," A.S.H.R.A.E. Journal, 1962, 4, pp. 52-60.

22. J. G. Collier, Convective Boiling and Condensation, McGraw-Hill Book Company, New York, 1972.

23. N. Zuber, M. Tribus and J. W. Westwater, "The Hydrodynamic Crisis in Pool Boiling of Saturated and Subcooled Liquids," International Developments in Heat Transfer, Part II, 1961, pp. 230-236.

24. L. Biasi, et al., "Studies on Burnout: Part 3," Energia Nucleare, 1967, 14, pp. 530-536.

25. Minutes of the Advanced Code Review Group Meeting, NRC Willste Building, Silver Springs, Maryland, January 25, 1980. Office of Research.

26. O. C. Iloeje and P. Griffith, "An Investigation of the Collapse and Surface Rewet in Film Boiling in Forced Vertical Flow," Transactions of ASME, pp. 166-172, May, 1975.

27. R. E. Henry, "A Correlation for the Minimum Film Boiling Temperature," AIChE Symposium Series 1974, 138, pp. 81-90.

28. R. Muralidaran, Editor, BWR Blowdown Heat Transfer Final Report, General Electric Company, February 1976 (GEAP-21214).

29. Lahey, R. T., Two-Phase Flow in Boiling Water Reactors, July 1974 (NEDO-13388).

30. P. Saha and N. Zuber, "Point of Net Vapor Generation and Vapor Void Fraction in Subcooled Boiling," Proceedings of the 5th International Heat and Mass Transfer Conference, Tokyo, Japan, 1974.

31. Jens G. M. Andersen and H. Abel-Larsen, CØRECØØL - Model Description of the Programme, Department of Reactor Technology, Riso National Laboratory, Denmark, November 1980 (RISØ-M-21380).

Appendix A

TWO-PHASE LEVEL STRATIFICATION

In the formulation of the momentum equations, it is assumed that the pressure is the same for each phase. This is usually correct for dispersed flow; however, for the case when a two-phase level exists (e.g., in the upper plenum), there may be significant differences in the pressure, particularly for large cells. For this case the assumption of same pressures for each phase can lead to unrealistic results. A simple modification to the momentum equation can, however, account for the difference in the pressures.

For dispersed flow the pressure at any point will be the same for each phase (neglecting surface tension effects, etc.), and the momentum equations for the x-direction (see Figure A-1) becomes

$$\alpha\rho_g \frac{dV_{gx}}{dt} = -\alpha \frac{\partial \overline{P}}{\partial x} - F_{\omega g} - f_{\ell g} \tag{A-1}$$

$$(1-\alpha)\ \rho_\ell \frac{dV_{\ell x}}{dt} = -(1-\alpha) \frac{\partial \overline{P}}{\partial x} - F_{\omega \ell} + f_{\ell g} \tag{A-2}$$

For stratified flow the pressures will not be the same for each phase. Neglecting inertia terms in the vertical direction, the average pressure for the mixture becomes

$$\overline{P}(x) = P_o(x) + \frac{L}{2}\ \rho_m\ (x)g \tag{A-3}$$

and the pressure of either phase becomes

$$P_g\ (x,z) = P_o(x) + \rho_g\ g(L-z) \tag{A-4}$$

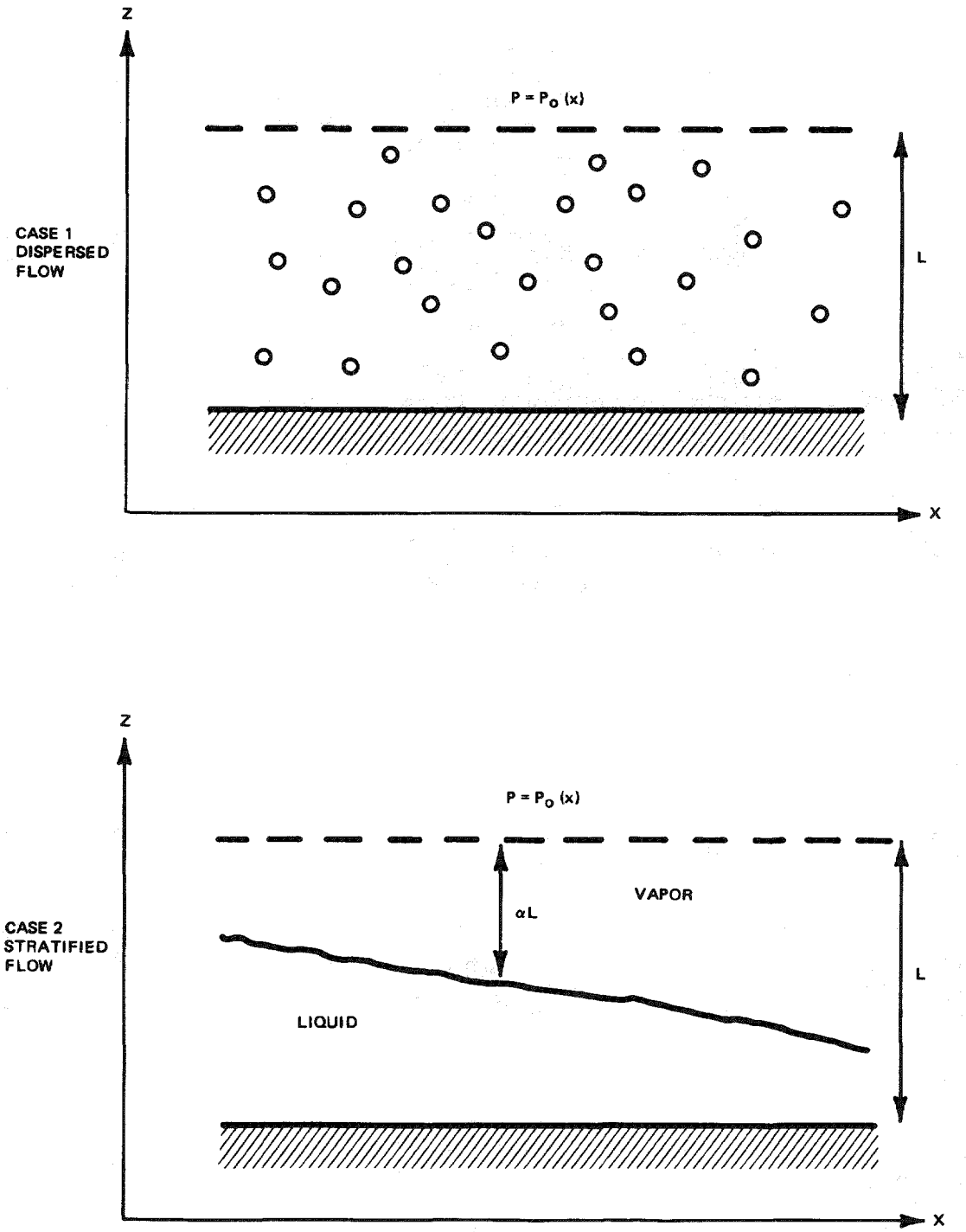

Figure A-1. Two-Phase Level Stratification

where

$$(1-\alpha)\ L \leq Z < L$$

$$P_\ell(x,z) = P_o(x) + \rho_g g\alpha L + \rho_\ell g\left((1-\alpha)L - z\right) \tag{A-5}$$

where

$$0 \leq Z < (1-\alpha)L$$

The horizontal pressure gradients are

$$\frac{\partial P_g}{\partial x} = \frac{\partial P_o}{\partial x} \tag{A-6}$$

$$\frac{\partial P_\ell}{\partial x} = \frac{\partial P_o}{\partial x} - \Delta\rho g L \frac{\partial \alpha}{\partial x} \tag{A-7}$$

Averaging over the cross section yields

$$\overline{\frac{\partial P_g}{\partial x}} = \frac{\partial P_o}{\partial x} \tag{A-8}$$

$$\overline{\frac{\partial P_\ell}{\partial x}} = \frac{\partial P_o}{\partial x} - \Delta\rho g L \frac{\partial \alpha}{\partial x} \tag{A-9}$$

Differentiating Equation A-3 gives

$$\frac{\partial \bar{P}}{\partial x} = \frac{\partial P_o}{\partial x} - \frac{L}{2}\Delta\rho g \frac{\partial \alpha}{\partial x} \tag{A-10}$$

which combined with Eqs. A-8 and A-9 gives:

$$\overline{\frac{\partial P_g}{\partial x}} = \frac{\partial \bar{P}}{\partial x} + \frac{L}{2}\Delta\rho g \frac{\partial \alpha}{\partial x} \tag{A-11}$$

$$\overline{\frac{\partial P_\ell}{\partial x}} = \frac{\partial \bar{P}}{\partial x} - \frac{L}{2}\Delta\rho g \frac{\partial \alpha}{\partial x} \tag{A-12}$$

and the momentum equations for the x-direction become

$$\alpha \rho_g \frac{dV_{gx}}{dt} = -\alpha \frac{\partial \overline{P}}{\partial x} - F_{\omega g} - f_{\ell g} - \alpha \frac{L}{2} \Delta\rho g \frac{\partial \alpha}{\partial x} \qquad \text{(A-13)}$$

$$(1-\alpha)\rho_\ell \frac{dV_{\ell x}}{dt} = -(1-\alpha) \frac{\partial \overline{P}}{\partial x} - F_{\omega \ell} + f_{\ell g} + (1-\alpha) \frac{L}{2} \Delta\rho g \frac{\partial \alpha}{\partial x} \qquad \text{(A-14)}$$

NRC FORM 335 (7-77)

U.S. NUCLEAR REGULATORY COMMISSION

BIBLIOGRAPHIC DATA SHEET

Do Not Microfilm

4. TITLE AND SUBTITLE *(Add Volume No., if appropriate)*

BWR Refill-Reflood Program, Task 4.7
Constitutive Correlations for Shear and Heat Transfer for the BWR Version of TRAC

7. AUTHOR(S)

J.G.M. Andersen and K.H. Chu

9. PERFORMING ORGANIZATION NAME AND MAILING ADDRESS *(Include Zip Code)*

General Electric Company
175 Curtner Avenue
San Jose, California 95125

MONTH: November YEAR: 1982

6. *(Leave blank)*

8. *(Leave blank)*

10. PROJECT/TASK/WORK UNIT NO.

11. CONTRACT NO.

Fin B5877

12. SPONSORING ORGANIZATION NAME AND MAILING ADDRESS *(Include Zip Code)*

U.S. Nuclear Regulatory Commission
Division of Reactor Safety Research
Office of Nuclear Regulatory Commission
Washington, D.C. 20555

13. TYPE OF REPORT

PERIOD COVERED *(Inclusive dates)*

15. SUPPLEMENTARY NOTES

14. *(Leave blank)*

16. ABSTRACT *(200 words or less)*

TRAC (Transient Reactor Analysis Code) is a computer code for best estimate analysis of the thermal hydraulic conditions in a reactor system. The constitutive correlations for shear and heat transfer in the boiling water reactor (BWR) version of TRAC are described.

A new model, that accounts for the effect of phase and velocity profiles, has been developed for the interfacial shear and a new set of constitutive correlations are derived. Improvements have been made to the heat transfer in the area of subcooled boiling, boiling transition, and thermal radiation.

17. KEY WORDS AND DOCUMENT ANALYSIS

17a. DESCRIPTORS

17b. IDENTIFIERS/OPEN-ENDED TERMS

18. AVAILABILITY STATEMENT

Unlimited

19. SECURITY CLASS *(This report)*: Unclassified

21. NO. OF PAGES

20. SECURITY CLASS *(This page)*

22. PRICE $

NRC FORM 335 (7-77)